Out-of-plane stability design of steel beams by second-order inelastic analysis with strain limits

Chunyan QUAN[1*], Merih KUCUKLER[2], Leroy GARDNER[1]

[1]*Department of Civil and Environmental Engineering, South Kensington Campus, Imperial College London, London SW7 2AZ, UK*

[2]*School of Engineering, University of Warwick, Coventry, CV4 7AL, UK*

* Corresponding author. E-mail address: c.quan17@imperial.ac.uk

Abstract:

An accurate and consistent approach to the out-of-plane stability design of steel beams and structures utilising second-order inelastic analysis with strain limits is proposed. The method is implemented using computationally efficient beam elements, with the ultimate structural resistance defined either by (i) the ultimate load factor or (ii) the load factor at which a strain limit, determined on the basis of the continuous strength method (CSM), is attained, whichever occurs first. Thus far, the method has been established for the in-plane design of steel structures and structural components; in the present paper, its scope is extended, for the first time, to the scenarios in which out-of-plane stability effects, with a focus on lateral-torsional buckling (LTB), govern. The accuracy and safety of the method are assessed against the results of nonlinear shell finite element (FE) modelling. It is shown that the proposed method consistently provides more accurate results than the traditional LTB design method of prEN 1993-1-1. In addition to its accuracy, the proposed approach also streamlines the design process by eliminating the need for cross-section classification and member design checks.

Keywords: Lateral-torsional buckling (LTB); Continuous strength method (CSM); Strain limits; Advanced inelastic analysis; Finite element modelling; Out-of-plane stability

1. INTRODUCTION

Steel structures and their components are often susceptible to out-of-plane instability effects, such as lateral-torsional buckling (LTB) – see Fig. 1. The influence of LTB on the resistance

of steel beams is generally accounted for in design standards by either: (i) the application of a buckling reduction factor to the cross-section bending resistance [1-4] or (ii) the determination of the elastic buckling moment of the beam with a reduced stiffness [5,6-13]. The former approach has traditionally been adopted in structural steel design standards [14-17] owing to its suitability for application through hand calculations [11] and its relative ease of extension to the design of beam-columns through the use of interaction curves [18-27]. However, the calculations required for considering the influence of bending moment diagram shapes on the spread of plasticity, the load height with respect to the shear centre and the interaction between adjacent laterally restrained segments of beams are somewhat drawn-out and often lead to rather inaccurate resistance predictions.

Geometrically and Materially Nonlinear Analysis with Imperfections (GMNIA), typically implemented using beam finite elements, is being increasingly employed in the design of steel structures. This approach brings a number of advantages, including (i) the need for carrying out individual member design checks can be avoided, (ii) global buckling behaviour (e.g. flexural buckling and LTB) can be directly and accurately captured and (iii) the structural failure modes can be explicitly visualised. Beam elements are highly computationally efficient, but are not able to capture the influence of local buckling on the cross-section resistance and rotation capacity of steel members. In current structural steel design codes, the influence of local buckling on the response of steel members is typically considered through the concept of cross-section classification, which restricts the cross-section resistance (e.g. plastic, elastic or effective moment capacity in bending) and the structural analysis type (i.e. plastic or elastic) on the basis of the classes of the cross-sections of the members making up the structure. However, this approach is not only overly-simplistic but also generates artificial steps in the resulting resistance predictions.

Recently, a new structural steel design approach utilising advanced analysis, together with the adoption of the continuous strength method (CSM) strain limits [28] to capture the influence of local buckling on the resistance of the cross-sections, has been put forward [29]. According to the proposed design approach, a GMNIA of the structure is performed using beam finite elements, considering explicitly buckling of the members and frame, the influence of imperfections and the spread of plasticity throughout the structure. The ultimate load carrying capacity of the structure is taken as either (i) the peak load factor obtained from the analysis α_{peak} or (ii) the load factor at which the CSM strain limit is attained α_{csm} at any cross-section in the considered member or structure, whichever occurs first. The accuracy and reliability of the proposed approach of design by GMNIA with strain limits have been verified for carbon steel [30,31] and stainless steel structures [32], considering a range of cases. However, the approach is currently limited to structures that are not susceptible to out-of-plane instability effects, thus limiting its scope of applicability.

In this paper, the approach is extended to cover the design of steel I-section beams against lateral-torsional buckling. A wide range of cases is considered, including variation in cross-section properties, member slendernesses and bending moment diagram shapes. Application of the proposed design approach to structural steel members subjected to pure torsion, combined bending and torsion, and combined shear, bending and torsion is also illustrated. The design capacity predictions are assessed relative to the results of benchmark shell FE models, which are themselves validated against existing experiments in the literature.

2. TRADITIONAL APPROACH FOR LTB ASSESSMENT OF STEEL BEAMS PROVIDED IN EN 1993-1-1 [14] AND PREN 1993-1-1 [15]

In this section, the traditional approach for the LTB assessment of steel beams given in EN 1993-1-1 [14] and prEN 1993-1-1 [15] is briefly described. EN 1993-1-1 [14] provides two

different sets of equations for the LTB assessment of steel beams. The first set of equations, referred to as the general case, are provided in Clause 6.3.2.2 and are applicable to beams with any cross-section type, while the second set of equations, referred to as the specific case, are provided in Clause 6.3.2.3 and are applicable to steel beams with I-shaped cross-sections. Since the focus of the present study is the LTB of I-section steel beams, only the specific case LTB assessment equations are described herein. LTB resistance $M_{\mathrm{b,Rd}}$ is expressed through Eq. (1):

$$M_{\mathrm{b,Rd}} = \chi_{\mathrm{LT}} \frac{M_{\mathrm{c,Rk}}}{\gamma_{\mathrm{M1}}} \tag{1}$$

where χ_{LT} is the buckling reduction factor, which considers the adverse effects of LTB on the in-plane (cross-section) resistance of the beam and $M_{\mathrm{c,Rk}}$ is the characteristic (unfactored) cross-section bending moment resistance equal to the product of yield stress f_{y} and the major axis section modulus W_{y} (i.e. $M_{\mathrm{c,Rk}} = W_{\mathrm{y}} f_{\mathrm{y}}$); W_{y} is taken as the plastic section modulus $W_{\mathrm{pl,y}}$ for Class 1 and 2 cross-sections, the elastic section modulus $W_{\mathrm{el,y}}$ for Class 3 cross-sections, and the effective section modulus $W_{\mathrm{eff,y}}$ for Class 4 cross-sections. The LTB reduction factor χ_{LT} is calculated using Eqs. (2)-(4):

$$\chi_{\mathrm{LT}} = \frac{1}{\phi_{\mathrm{LT}} + \sqrt{\phi_{\mathrm{LT}}^2 - \beta \bar{\lambda}_{\mathrm{LT}}^2}} \leq \min(1,\ 1/\bar{\lambda}_{\mathrm{LT}}^2) \tag{2}$$

$$\phi_{\mathrm{LT}} = 0.5\left[1 + \alpha_{\mathrm{LT}}\left(\bar{\lambda}_{\mathrm{LT}} - \bar{\lambda}_{\mathrm{LT,0}}\right) + \beta \bar{\lambda}_{\mathrm{LT}}^2\right] \tag{3}$$

$$\bar{\lambda}_{\mathrm{LT}} = \sqrt{M_{\mathrm{c,Rk}} / M_{\mathrm{cr}}} \tag{4}$$

where α_{LT} is the imperfection factor determined on the basis of the cross-section depth to width ratios, as explained in EN 1993-1-1 [14], β is a modification factor, $\bar{\lambda}_{\mathrm{LT}}$ is the normalised slenderness, $\bar{\lambda}_{\mathrm{LT,0}}$ is the threshold slenderness and M_{cr} is the elastic critical buckling moment. To take account of the influence of non-uniform bending on ultimate resistance, the LTB

reduction factor may be modified using Eq. (5), where k_c is a correction factor given in EN 1993-1-1 [14] for different bending moment diagram shapes.

$$\chi_{\mathrm{LT,mod}} = \frac{\chi_{\mathrm{LT}}}{1-0.5\left(1-k_{\mathrm{c}}\right)\left[1-2\left(\bar{\lambda}_{\mathrm{LT}}-0.8\right)^2\right]} \tag{5}$$

In the upcoming version of EN 1993-1-1 [14], referred to herein as prEN 1993-1-1 [15], the bending moment resistance of I-section steel beams undergoing LTB are again calculated using Eq. (1), but the equations used to determine χ_{LT} have been improved, as given by Eqs. (6)-(7),

$$\chi_{\mathrm{LT}} = \frac{f_{\mathrm{M}}}{\phi_{\mathrm{LT}} + \sqrt{\phi_{\mathrm{LT}}^2 - f_{\mathrm{M}}\bar{\lambda}_{\mathrm{LT}}^2}} \leq 1 \tag{6}$$

$$\phi_{\mathrm{LT}} = 0.5\left[1 + f_{\mathrm{M}}\left(\left(\frac{\bar{\lambda}_{\mathrm{LT}}}{\bar{\lambda}_{\mathrm{z}}}\right)^2 \alpha_{\mathrm{LT}}\left(\bar{\lambda}_{\mathrm{z}} - 0.2\right) + \bar{\lambda}_{\mathrm{LT}}^2\right)\right] \tag{7}$$

where f_{M} is a factor that accounts for the influence of bending moment gradient and $\bar{\lambda}_{\mathrm{z}}$ is the normalised member slenderness for minor axis flexural buckling. Note that the definition of the imperfection factor α_{LT} was also amended, becoming a function of the major $W_{\mathrm{el,y}}$ and minor axis $W_{\mathrm{el,z}}$ elastic section moduli of the beam cross-section.

The influence of local buckling on the cross-section resistances of steel members is considered through the cross-section classification concept [14-16]. According to this concept, a cross-section is classified into one of three (compact, non-compact and slender) [16] or four (Class 1, Class 2, Class 3 and Class 4) classes [14,15], based on its susceptibility to local buckling. Although straightforward to apply, the cross-section classification concept has a number of shortcomings, including (i) taking no account of the beneficial effect of the interaction between the individual plate elements making up the cross-section during local buckling [33], (ii) neglect or over-simplistic treatment of the influence of partial plasticity in Class 3 cross-sections, (iii) failure to consider material strain hardening in the determination of the ultimate

resistances of stocky cross-sections and (iv) taking no account of the beneficial effect of non-uniform bending moment gradients along the lengths of steel members on their local cross-section stability [30,31,34], as explained in Section 3.3.

3. DESIGN OF STEEL BEAMS BY ADVANCED INELASTIC ANALYSIS USING BEAM ELEMENTS WITH CSM STRAIN LIMITS

The proposed method of design by second-order inelastic analysis with strain limits involves: (i) carrying out a GMNIA of the steel member using beam finite elements and (ii) using the load factor that corresponds to the attainment of the peak load α_{peak} or the CSM strain limit α_{csm}, whichever occurs first, to define the ultimate resistance. Development of the primary components of the proposed design method for the out-of-plane stability assessment of steel beams is explained in this section.

3.1 The continuous strength method (CSM): strain limits, cross-section slenderness and material model

The continuous strength method (CSM) is a deformation-based design approach that establishes a relationship between the ultimate deformation capacity of a cross-section and its local slenderness. The CSM was proposed by Gardner [28] and has been applied to the design of stainless steel [35,36], carbon steel [37,38] and aluminium alloy [39-41] structural members, as well as planar steel frames [30]. The CSM has two key features: (i) a base curve that defines the maximum strain ε_{csm} that a cross-section can experience prior to its failure, with ε_{csm} presented relative to the yield strain ε_y and presented as a function of the cross-section slenderness $\bar{\lambda}_p$ and (ii) an appropriate constitutive model describing the stress-strain response of the structural material. The CSM can be used as an alternative to the cross-section classification concept and enables a more consistent and continuous treatment of the influence

of local instability effects on the ultimate resistances of cross-sections ranging from Class 1 to Class 4.

As shown in Fig. 2, the CSM base curve is split into two parts, and the transition point between the two parts, distinguishing between non-slender and slender cross-sections, is set at $\bar{\lambda}_p = 0.68$ [36]. For non-slender cross-sections ($\bar{\lambda}_p \leq 0.68$), the CSM strain limit, given by Eq. (8), is greater than or equal to the yield strain (i.e. $\varepsilon_{csm}/\varepsilon_y \geq 1$), allowing for the rational exploitation of the development and spread of plasticity and strain hardening:

$$\frac{\varepsilon_{csm}}{\varepsilon_y} = \frac{0.25}{\bar{\lambda}_p^{\,3.6}} \quad \text{but } \leq \Omega \quad \text{for } \bar{\lambda}_p \leq 0.68 \tag{8}$$

where the upper limit Ω is a project specific design parameter that defines the maximum permitted level of plastic deformation, for which the value of 15 is recommended, complying with the ductility requirement given for structural steel in EN 1993-1-1 [14]. A second upper limit to Eq. (8) is required when simplified resistance functions, suitable for hand calculations [37], are employed, but is not needed in design by advanced analysis when the full material stress-strain curve is defined, as described below.

For slender cross-sections ($0.68 < \bar{\lambda}_p \leq 1.0$), the CSM strain limit, given by Eq. (9), is less than the yield strain (i.e. $\varepsilon_{csm}/\varepsilon_y < 1$):

$$\frac{\varepsilon_{csm}}{\varepsilon_y} = \left(1 - \frac{0.222}{\bar{\lambda}_p^{\,1.05}}\right)\frac{1}{\bar{\lambda}_p^{\,1.05}} \qquad \text{for } 0.68 < \bar{\lambda}_p \leq 1.0 \tag{9}$$

In Eqs. (8) and (9), the cross-section slenderness $\bar{\lambda}_p$ is determined using Eq. (10), where f_y is the material yield stress and $\sigma_{cr,cs}$ is the elastic local buckling stress of the full cross-section, which can be calculated numerically (e.g. through the finite strip software *CUFSM* [42]), or using the simplified formulae developed by Gardner et al. [33].

$$\bar{\lambda}_{\mathrm{p}} = \sqrt{\frac{f_{\mathrm{y}}}{\sigma_{\mathrm{cr,cs}}}} \tag{10}$$

The second key feature of the CSM is the definition of an accurate and appropriate material model. In this study, the quad-linear stress-strain model for hot-rolled steels developed by Yun and Gardner [43] was used. This material model has been shown to provide a very accurate representation of the stress-strain response of different steel grades and is illustrated in Fig. 3. Unless otherwise indicated, grade S355 steel has been used in all the cases considered in this study; thus, the three required parameters for the material model of [43] were taken as the Young's modulus E = 210000 MPa, the yield stress f_{y} = 355 MPa and the ultimate stress f_{u} = 510 MPa. The stress-strain relationship over the full range is defined by:

$$\sigma = \begin{cases} E\varepsilon & \text{for } \varepsilon \le \varepsilon_{\mathrm{y}} \\ f_{\mathrm{y}} & \text{for } \varepsilon_{\mathrm{y}} < \varepsilon \le \varepsilon_{\mathrm{sh}} \\ f_{\mathrm{y}} + E_{sh}\left(\varepsilon - \varepsilon_{\mathrm{sh}}\right) & \text{for } \varepsilon_{\mathrm{sh}} < \varepsilon \le C_1\varepsilon_{\mathrm{u}} \\ f_{C_1\varepsilon_{\mathrm{u}}} + \dfrac{f_{\mathrm{u}} - f_{C_1\varepsilon_{\mathrm{u}}}}{\varepsilon_{\mathrm{u}} - C_1\varepsilon_{\mathrm{u}}}\left(\varepsilon - C_1\varepsilon_{\mathrm{u}}\right) & \text{for } C_1\varepsilon_{\mathrm{u}} < \varepsilon \le \varepsilon_{\mathrm{u}} \end{cases} \tag{11}$$

where the strain $\varepsilon_{\mathrm{sh}}$ at which strain hardening begins, the ultimate strain ε_{u} and the strain hardening modulus E_{sh} are defined by Eqs. (12)-(14) respectively.

$$\varepsilon_{\mathrm{sh}} = 0.1\frac{f_{\mathrm{y}}}{f_{\mathrm{u}}} - 0.055 \qquad \text{but } 0.015 \le \varepsilon_{\mathrm{sh}} \le 0.03 \tag{12}$$

$$\varepsilon_{\mathrm{u}} = 0.6\left(1 - \frac{f_{\mathrm{y}}}{f_{\mathrm{u}}}\right) \qquad \text{but } \varepsilon_{\mathrm{u}} \ge 0.06 \tag{13}$$

$$E_{\mathrm{sh}} = \frac{f_{\mathrm{u}} - f_{\mathrm{y}}}{C_2\varepsilon_{\mathrm{u}} - \varepsilon_{\mathrm{sh}}} \tag{14}$$

Finally, in the adopted material model, the constants C_1 and C_2 are given by Eqs. (15) and (16).

$$C_1 = \frac{\varepsilon_{\mathrm{sh}} + 0.25\left(\varepsilon_{\mathrm{u}} - \varepsilon_{\mathrm{sh}}\right)}{\varepsilon_{\mathrm{u}}} \tag{15}$$

$$C_2 = \frac{\varepsilon_{\mathrm{sh}} + 0.4\left(\varepsilon_{\mathrm{u}} - \varepsilon_{\mathrm{sh}}\right)}{\varepsilon_{\mathrm{u}}} \tag{16}$$

3.2 FE modelling of steel structures using beam finite elements

The proposed design method is implemented using beam finite elements. In this study, the finite element analysis software Abaqus [44] was used to carry out the GMNIA simulations. The shear deformable prismatic Timoshenko beam element referred to as B31OS in Abaqus [44], which is capable of modelling the effects of torsion and warping in open-sections, was used. Thirty-three section integration points were employed along the widths of each web and flange plate to accurately capture the spread of plasticity through the cross-section. To enable the application of the strain averaging approach [31], which is used to take account of the beneficial influence of local strain gradients along the member lengths on cross-section resistance, as described in the next subsection, the lengths of the beam elements were defined to be less than or equal to the corresponding local buckling half-wavelengths $L_{b,cs}$ of the cross-sections of the modelled beams. The quad-linear material model introduced in the previous subsection was employed, with the engineering stress-strain curve converted in true stress and strain. Nominal values of material strengths and geometries, together with the characteristic value of the Young's modulus (E = 200000 MPa [15]) were employed in the implementation of the proposed design approach, as recommended in [32,45]. The combined influence of the geometric imperfections and residual stresses was accounted for through the use of equivalent geometric imperfections [15], as is recommended for the practical implementation of the proposed design method. The equivalent imperfections were modelled through the scaling of the first LTB eigenmode with the amplitude proposed in a parallel study [46] on the out-of-plane design of steel members by GMNIA. In this paper, all the investigated steel beams had fork-end support conditions, allowing warping deformations but fully restraining twisting about the longitudinal axis of the members at the supports.

3.3 Procedure for application of CSM strain limits in GMNIA

Using GMNIA with beam finite elements, global member instabilities can be captured directly, but local cross-section instabilities cannot. Thus, in [31], it was proposed that the CSM strain limits are applied to account for the influence of local buckling on the response; this is implemented by checking the maximum compressive longitudinal strains against the corresponding CSM strain limits for all cross-sections in the structure at each load increment, with the critical section governing the overall design.

In previous research [47-52], it has been observed that steel beams subjected to bending moment gradients exhibit greater cross-section resistances than beams with the same geometric and material properties but under uniform bending. This was ascribed to the beneficial effect of local strain gradients along the member lengths on the local stability of cross-sections [31,53], i.e. the critical cross-sections receive support from the adjacent less heavily loaded cross-sections. It was shown in [31] that this effect could be accurately captured by averaging the maximum compressive longitudinal (normal) strains in the cross-sections over a defined length and limiting the averaged strains (rather than the peak strains) to the CSM strain limits. The defined averaging length is taken as the elastic local buckling half-wavelengths $L_{b,cs}$ [31] which can be obtained numerically, e.g. using the finite strip method software *CUFSM* [42], or through the expressions presented in [54].

For steel I-section beams susceptible to lateral-torsional buckling, internal second-order torsion arises upon the application of the major axis bending moments. The total internal torsion moment T_{Ed} at any given cross-section has two components: (i) the St. Venant torsion T_{St} with associated St. Venant torsion shear stresses τ_{St} and (ii) the warping torsion T_w with associated warping torsion normal stresses σ_w and warping torsion shear stresses τ_w, as shown in Fig. 4. In the implementation of the proposed design method by the GMNIA of steel beams with beam finite elements, the normal strains ε_w resulting from the warping torsion normal stresses σ_w can

be directly extracted and the total maximum compressive normal strains within cross-sections due to the combination of bending and warping can be checked against the CSM strain limits. However, the St. Venant torsion τ_{St} and the warping torsion shear stresses τ_w still need to be considered; the treatment of shear stresses arising from either primary or secondary torsion in the proposed design method is provided in Section 6.

As shown in Fig. 5, the procedure for the application of the proposed design approach to steel beams susceptible to LTB is as follows:

I. Based on the first-order internal force distribution, determine the elastic local buckling stresses of the cross-sections $\sigma_{cr,cs}$ at the middle of each element along the beam length [33,42].

II. Using Eq. (10), calculate the corresponding cross-section slendernesses $\bar{\lambda}_p$.

III. Using the calculated $\bar{\lambda}_p$ values, determine the strain limits ε_{csm} for the cross-sections at the middle of each element using the CSM base curve given by Eqs. (8) and (9). For elements under high shear force and/or torsion, reduce the strain limits considering the shear effect from shear force and/or torsion (see Sections 5.2 and 6.1.3).

IV. If the strain averaging approach is used, calculate the local buckling half-wavelengths of the cross-sections $L_{b,cs}$ on the basis of the first-order internal force distribution, either using numerical methods (e.g. *CUFSM* [42]) or the expressions provided in [54] and determine the average maximum compressive normal strain for each element $\varepsilon_{Ed,av,m}$ as the average of the peak compressive strains $\varepsilon_{Ed,m}$ over the local buckling half-wavelengths $L_{b,cs}$, as shown in Fig. 6. Note that in the calculation of $\varepsilon_{Ed,av,m}$, only the elements that lie fully within $L_{b,cs}$ should be considered.

V. Determine (i) the load increment j (if any) at which the peak load factor is reached and (ii) the load increment p at which the average strain at any cross-section m_0 attains the CSM

strain limit, i.e. $\varepsilon_{Ed,av,m_0,p} \geq \varepsilon_{csm}$ or $\varepsilon_{Ed,av,m_0,p} \geq \rho_{csm,m_0}\varepsilon_{csm}$ or ε_{csm,V,m_0} for members under high shear and/or torsion (reduction is applied to the CSM strain limit ε_{csm} for the latter – see Sections 5.2 and 6.1.3). If j is less than p, the member is deemed to fail primarily due to global instability i.e. lateral-torsional buckling, and the characteristic resistance factor α_{Rk} is taken as the peak load factor from the GMNIA α_{peak} (i.e. $\alpha_{Rk} = \alpha_{peak}$); otherwise, the member is deemed to fail by attaining the cross-section capacity, and the load factor at which the CSM strain limit is attained α_{csm} is adopted as the characteristic resistance factor α_{Rk} (i.e. $\alpha_{Rk} = \alpha_{csm}$).

VI. As recommended in [15,32,45], in the implementation of the proposed design method, the Young's modulus should be taken as the characteristic value of E = 200000 MPa, and the resulting resistance should be assumed to be the characteristic resistance, to which a partial safety factor (γ_{M1} = 1.0) should be applied. Hence, finally, the design resistance factor of the member α_{Rd} is equal to the characteristic resistance factor α_{Rk} divided by the partial safety factor γ_{M1}, as given by Eq. (17).

$$\alpha_{Rd} = \alpha_{Rk} / \gamma_{M1} \tag{17}$$

4. BENCHMARK SHELL FINITE ELEMENT MODELLING

4.1 Modelling approach

In this paper, the accuracy of the proposed design approach for the LTB assessment of steel beams is verified against the results from shell FE modelling considering various cross-section proportions, member slendernesses and loading conditions. The shell finite element models were created using the finite element analysis software Abaqus [44]. The four-noded general purpose S4R shell element, taking into account transverse shear deformations and finite membrane strains with reduced integration and a large-strain formulation, which has been successfully employed in previous studies for similar applications [31,55-58], was used to create all the models. Each web and flange plate of the cross-sections was subdivided into 16

elements. The number of elements along the member lengths was defined such that the element aspect ratios were close to unity. The Simpson integration method was adopted, and five integration points were employed through the thickness of the shell elements [44].

The quad-linear stress-strain model developed by Yun and Gardner [43] for hot-rolled steel was employed to define the material stress-strain response. The Poisson's ratio was taken as $\nu = 0.3$ in the elastic range and $\nu = 0.5$ in the plastic range. As required by Abaqus [44], the engineering stress-strain relationships were transformed into true stress-strain curves.

Beam multi-point constraints were employed to connect the web and two flange plates making up the cross-sections of the investigated members. To avoid overlapping of the web and flange plates, the web plates were offset by half the flange thicknesses, in line with the approach adopted in [11,12,55]. Fork-end support conditions enabling warping deformations but preventing twist were applied at the member ends by the application of coupling constraints. The ECCS [59] residual stress pattern for hot-rolled steel sections illustrated in Fig. 7 (a) was adopted in the shell finite element models. Unless otherwise indicated, initial geometric imperfections in the shape of the first LTB eigenmode with an amplitude of 1/1000 of the unbraced lengths were incorporated into the FE models. As shown in Fig. 7 (b), local geometric imperfections were also applied to the shell finite element models by adopting a series of sinusoidal subpanel imperfections, complying with the recommendations provided in Annex C of EN 1993-1-5 [60]. For the cases where the web plate was more susceptible to local buckling than the flange plates, i.e. when $\sigma_{cr,w} < \sigma_{cr,f}$ (where $\sigma_{cr,w}$ and $\sigma_{cr,f}$ are the elastic local buckling stresses of the isolated web and flange plates assuming simply-supported boundary conditions), the magnitude of the local web imperfection was taken as 1/200 of the web heights h_w (i.e. $h_w/200$). Similarly, for the cases where the flange plates were more susceptible to local buckling than the web plate, the magnitudes of the local flange imperfections were taken as 1/100 of the flange widths b (i.e. $b/100$). The local imperfection magnitudes of the non-critical plate

elements were defined such that the web-to-flange junctions remained at 90°. The local geometric imperfections were applied to the shell FE models using the local buckling half-wavelengths $L_{b,cs}$, which were obtained from the expressions provided in [54]. It should be noted that in the case of some members with very short span lengths, the shell FE models did not exhibit a peak load; in these cases, the failure was defined when the tangent stiffness of the model degraded to 1% of its initial stiffness, similar to the approach proposed by [61] and adopted in [31].

4.2 Validation of shell FE models

The shell FE models developed in this study were validated against the results from 59 experiments on beams experiencing LTB collected from the literature [62-69]. The loading configurations included (i) 3-point bending and 4-point bending [62], (ii) concentrated loading applied at the free-end of cantilever beams [63,64] and (iii) 3-point bending with eccentrically applied vertical loading, leading to additional torsion [65-69]. The boundary and loading conditions employed in the tests were replicated in the FE models. The geometric imperfection was modelled through the scaling of the first LTB eigenmode. Where reported, the measured global geometric imperfection amplitudes were incorporated into the FE models. For the cases where the geometric imperfection magnitudes were not reported, a magnitude of 1/1000 of the laterally unbraced lengths were used. A summary of the validation study, including the mean and coefficient of variation (CoV) values of the ratios of the ultimate load carrying capacities determined using the shell FE models $\alpha_{u,shell}$ to those obtained from the experiments $\alpha_{u,test}$ (i.e. $\alpha_{u,shell}/\alpha_{u,test}$), is given in Table 1. As can be seen from the table, the shell FE models created in this study are able to provide ultimate strength predictions that are very close to those observed in the physical experiments.

In Fig. 8, the experimental and numerical load-vertical displacement and load-twist curves for a sample of the beams tested under eccentric 3-point bending in [65] and [66,67] are shown,

where P is the applied load, w and ϕ are the vertical displacement and twist at the midspan respectively and $P_{\mathrm{u,test}}$ is the ultimate load obtained from the experiments. As can be seen from the figures, the numerical load-deformation paths obtained from the shell FE models closely follow the load-deformation paths observed in the experiments, indicating that the shell finite element models created in this paper are able to accurately replicate the structural response of steel beams undergoing LTB and can be used to generate benchmark data to evaluate the accuracy and safety of the proposed design approach.

5. ACCURACY OF PROPOSED DESIGN METHOD FOR STEEL BEAMS SUSCEPTIBLE TO LTB

In this section, the accuracy of the proposed design method is assessed against the benchmark results obtained from shell FE modelling for steel beams subjected to uniform and non-uniform bending. For comparison, the accuracy of the traditional design method provided in prEN 1993-1-1 [15] for the LTB assessment of steel beams is also investigated.

5.1 Beams under uniform bending

The accuracy of the proposed design approach is assessed for steel I-section beams under uniform bending in this subsection, covering a broad range of normalised member LTB slenderness values $0.2 \leq \bar{\lambda}_{\mathrm{LT}} = \sqrt{M_{\mathrm{c,Rk}} / M_{\mathrm{cr}}} \leq 1.8$ and a large number of different cross-section geometries including 10 IPE, 10 HEB and 10 HEA European profiles, where the cross-section slendernesses $\bar{\lambda}_{\mathrm{p}}$ ranged between 0.26 and 0.60 (i.e. $0.26 \leq \bar{\lambda}_{\mathrm{p}} = \sqrt{f_{\mathrm{y}} / \sigma_{\mathrm{cr,cs}}} \leq 0.60$).

Fig. 9 shows an illustrative example of the application of the proposed method to a steel beam with an HEA 260 cross-section under uniform bending. The normalised moment-outer fibre compressive strain response from the shell and beam FE models are displayed in Fig. 9. In the figure, the applied end bending moment M is normalised by the major axis plastic moment

capacity of the cross-section $M_{pl,y}$ (i.e. $M/M_{pl,y}$), while the strain is the average maximum compressive strain over the local buckling half-wavelength for the critical beam element m_0 (which is the element at the midspan in this case) ε_{Ed,av,m_0} normalised by the yield strain ε_y. In the beam element model, the average strain at the midspan reaches the CSM strain limit ε_{csm} = $1.65\varepsilon_y$ prior to the attainment of the peak load factor. Thus, this member is deemed to fail when the allowable CSM strain limit is reached, with a corresponding bending moment capacity $M_{u,prop}$ = $0.476M_{pl,y}$. The corresponding benchmark shell FE model reached a maximum bending moment of $M_{u,shell}$ = $0.480M_{pl,y}$ following the occurrence of local buckling of the compression flange at midspan, which is only 0.8% higher than the ultimate bending moment resistance determined using the proposed method $M_{u,prop}$, illustrating the very high accuracy of the proposed design approach. Note that if cross-section failure, as defined by the CSM strain limit, were to have been ignored, an unconservative prediction of the bending resistance, as given by the peak moment from the beam element model of M_{peak} = $0.513M_{pl,y}$ would have been obtained. The ultimate bending capacity predicted by the traditional design method in prEN 1993-1-1 [15] $M_{u,EC3}$ = $0.392M_{pl,y}$ is conservative, 18% lower than the benchmark shell FE result. Note also that in this example and all the considered cases in this study, the strain outputs and CSM strain limits are determined at the centreline of the wall thicknesses of the modelled I-sections, as described in detail in [31].

Fig. 10 shows the normalised ultimate bending capacities $M_u/M_{pl,y}$ of all considered 300 steel beams undergoing LTB determined through the benchmark shell FE models, the proposed design method and prEN 1993-1-1 [15] for different LTB slendernesses $\bar{\lambda}_{LT}$. With increasing LTB slendernesses $\bar{\lambda}_{LT}$, steel beams become more susceptible to LTB and exhibit lower ultimate bending moment resistances.

In Fig. 11, the ultimate bending moment resistances M_u of the considered range of steel beams predicted using the proposed design method and prEN 1993-1-1 [15] are compared against those obtained from the GMNIA of the benchmark shell FE models $M_{u,shell}$. As shown in Fig. 11 (a) and Table 2, the proposed method is able to provide very accurate capacity predictions – the mean value of the ratios of the ultimate resistances determined through the proposed method $M_{u,prop}$ to those determined from the shell FE models $M_{u,shell}$ (i.e. $M_{u,prop}/M_{u,shell}$) is equal to 0.984 with a CoV value of 0.016. On the other hand, prEN 1993-1-1 [15] yields less accurate and more scattered predictions, with a mean value of 0.901 and a CoV value of 0.137 for the ratios of ultimate resistances determined using prEN 1993-1-1 [15] to those obtained from the shell finite element models. Note that prEN 1993-1-1 [15] leads to some rather unsafe results for beams with $\bar{\lambda}_{LT}$ = 0.4 and some overly conservative results for slender members (e.g. $\bar{\lambda}_{LT}$ ≥ 1.4), as shown in Fig. 11 (b).

5.2 Beams under moment gradients

In addition to steel beams under uniform bending, the accuracy of the proposed design method is also assessed for 1200 steel beams undergoing LTB and subjected to different bending moment gradients along their lengths. As summarised in Table 2, the following parameters were considered: (i) the ratio of the bending moments applied at the beam ends ψ equal to 0.5, 0, -0.5 and -1 (i.e. ψ = 0.5, 0, -0.5 and -1), (ii) the normalised LTB slenderness $\bar{\lambda}_{LT}$, ranging between 0.25 and 1.40 (i.e. $0.25 \leq \bar{\lambda}_{LT} \leq 1.40$), and (iii) the cross-section geometry, by considering 10 IPE, 10 HEB and 10 HEA European profiles, thereby covering a broad range of cross-section slenderness values $\bar{\lambda}_p$ between 0.26 and 0.60 (i.e. $0.26 \leq \bar{\lambda}_p \leq 0.60$).

A bending moment gradient within a steel beam leads to the development of vertical shear forces along its length; the presence of high shear forces may adversely influence the bending moment capacity of the beam. To allow for this effect, the approach proposed in [31] was

adopted in this study; thus, when the design shear force $V_{y,Ed}$ exceeds half the plastic major axis shear resistance of the cross-section $V_{pl,y}$, the interaction between bending and shear is accounted for through a reduction factor ρ_{csm} applied to the CSM strain limit. The expression for the determination of the reduction factor ρ_{csm} is given by Eqs. (18)-(19). Note that separate cross-section shear capacity and shear buckling checks are still required in the application of the proposed design method, which can be carried out using the relevant provisions of EN 1993-1-1 [14] and EN 1993-1-5 [60]. Even though there exist lateral (minor axis) shear forces within the cross-sections of steel beams experiencing LTB, it was observed that these shear forces are consistently very small in the large number of steel beams considered in this paper. Thus, no reduction to the CSM strain limits due to the presence of high minor axis shear forces is considered necessary in practical LTB design situations.

$$\rho_{csm} = \begin{cases} 1 & \text{for } V_{y,Ed} \le 0.5V_{pl,y} \\ \dfrac{0.5}{0.5+\rho} & \text{for } V_{y,Ed} > 0.5V_{pl,y} \end{cases} \tag{18}$$

$$\rho = \left(\frac{2V_{y,Ed}}{V_{pl,y}} - 1 \right)^2 \tag{19}$$

Comparisons of the ratios of the ultimate bending moment capacities predicted by the proposed design method and prEN 1993-1-1 [15] to those determined from the benchmark shell FE models for members under different shapes of bending moment diagrams are shown in Fig. 12. Both limiting failure conditions i.e. attainment of the peak load factor and the CSM strain limits were exhibited among the analysed cases. Fig. 12 shows that the proposed design method generally provides very accurate and safe-sided resistance predictions for different cross-section slendernesses $\bar{\lambda}_p$. As presented in Fig. 12 and Table 2, relative to prEN 1993-1-1 [15], the proposed design method offers an average improvement of approximately 8% in accuracy, as well as a consistent reduction in the scatter of the predictions. As shown in Fig. 13, for beams

with relatively high member slendernesses (e.g. $\bar{\lambda}_{LT} \geq 1.0$), prEN 1993-1-1 [15] provides overly-conservative resistance predictions, with the predictions becoming increasingly conservative with increasing beam slendernesses $\bar{\lambda}_{LT}$; prEN 1993-1-1 [15] is also overly-conservative for stocky members (e.g. $\bar{\lambda}_{LT} \leq 0.6$) due to the neglect of the influence of material strain hardening on the ultimate resistances. By contrast, as shown in Fig. 14, the proposed design method offers considerably improved accuracy by allowing for the beneficial influence of both material strain hardening and local bending moment gradients on cross-section capacity.

The influence of the adoption of the strain averaging approach on the accuracy of the resistance predictions obtained using the proposed design method is explored in Fig. 15; this figure shows the ratios of the predicted ultimate bending capacities obtained from the proposed design method adopting the strain averaging approach $M_{u,prop}$ ($\varepsilon_{Ed,av}$) and without employing strain averaging $M_{u,prop}$ (ε_{Ed}) (i.e. $M_{u,prop}$ ($\varepsilon_{Ed,av}$)/$M_{u,prop}$ (ε_{Ed})) for steel beams subjected to different bending moment gradients and failing due to the attainment of the CSM strain limits. In typical I-section steel beams, relative to the normal strains resulting from the applied major axis bending moments, the normal strains caused by second-order warping torsion and second-order minor axis bending moments, which vary along the member lengths, are small. Thus, as can be seen in Fig. 15, for members under uniform bending (i.e. $\psi = 1$), the strain averaging approach does not have a significant influence on the ultimate resistance predictions, since there is no variation in the major axis bending moments along the member lengths; only the second-order warping torsion and the second-order minor axis bending moments vary along the member lengths, and their influence on the development of the normal strains is considerably lower than that of the major axis bending. On the other hand, for steel beams subjected to non-uniform major axis bending, applying the strain averaging approach leads to enhanced ultimate bending

moment resistance predictions, which can be up to 14% higher than those determined without adopting the strain averaging approach.

As previously indicated, high shear forces can adversely affect the bending resistances of steel beams. In Fig. 16, comparisons between the ultimate bending moment resistances determined through the proposed design method with or without the application of the shear force reduction factor ρ_{csm} to the CSM strain limits are presented, considering the cases where the shear forces within the beams exceeded half of their cross-section shear resistances $V_{u,prop}/V_{pl,y} > 0.5$; note that in all the cases, failure was due to the attainment of the CSM strain limits in the beams. As can be seen from Fig. 16, if the adverse influence of the high shear forces on the bending capacities is ignored, the predictions obtained from the proposed method can become unconservative. On the other hand, if the reduction factor ρ_{csm} is applied to the CSM strain limits for the cases where $V_{y,Ed}/V_{pl,y} > 0.5$, the unconservative predictions shift to the safe side, indicating the importance of applying the shear force reduction factor ρ_{csm} to the CSM limits for steel beams where the shear forces exceed half of the cross-section shear resistances $V_{y,Ed}/V_{pl,y} > 0.5$.

6. CONSIDERATION OF TORSION IN THE PROPOSED DESIGN METHOD

In steel structures, pure torsion is relatively unusual; typically, torsion arises in steel members in combination with bending. As indicated in Section 3.3, in the implementation of the proposed design method, normal strains ε_w resulting from warping torsion normal stresses can be included in the total normal strains that can be directly extracted from the analysis and checked against the CSM strain limits. However, in this approach, the influence of St. Venant torsion τ_{St} and warping torsion shear stresses τ_w is not directly considered. The consideration of these shear effects due to (first or second order) torsion in the application of the proposed design method is described in this section.

6.1 Proposed approach for the consideration of torsion effects

6.1.1 Internal torsion effects and torsional resistances of steel cross-sections

In the proposed design approach, St. Venant torsion and warping torsion shear effects are taken into account through considering the ratios of the internal St. Venant torsion $T_{\mathrm{St,Ed}}$ to the cross-section St. Venant torsion resistance $T_{\mathrm{St,Rk}}$ (i.e. $T_{\mathrm{St,Ed}}/T_{\mathrm{St,Rk}}$) and the internal warping torsion $T_{\mathrm{w,Ed}}$ to the cross-section warping torsion resistance $T_{\mathrm{w,Rk}}$ (i.e. $T_{\mathrm{w,Ed}}/T_{\mathrm{w,Rk}}$). Since the total internal torsion T_{Ed} within steel members can be directly extracted from GMNIA using beam finite elements, but some FE software packages (e.g. Abaqus [44]) do not enable the extraction of the individual St. Venant $T_{\mathrm{St,Ed}}$ and warping $T_{\mathrm{w,Ed}}$ torsion components, the use of Eq. (20) and Eq. (21) is recommended for the determination of the internal St. Venant $T_{\mathrm{St,Ed}}$ and warping torsion $T_{\mathrm{w,Ed}}$ within steel elements, respectively [15].

$$T_{\mathrm{St,Ed}} = GI_{\mathrm{t}}\phi' \tag{20}$$

$$T_{\mathrm{w,Ed}} = T_{\mathrm{Ed}} - T_{\mathrm{St,Ed}} \tag{21}$$

In Eq. (20), G is the shear modulus, I_{t} is the St. Venant torsion constant, and ϕ' is the first derivative of twist with respect to distance along the member length, which can be approximately taken as the ratio of the difference of the twists ϕ at the two end nodes of a beam element $\Delta\phi$ to the element length l (i.e. $\phi' = \Delta\phi/l$). The accuracy of this approximate approach is presented in Fig. 17. As can be seen from the figure, for all pure torsion, pure bending and combined bending and torsion cases, the warping moments determined from beam FE models using the proposed approximate approach agree well with the values obtained from shell FE models.

For St. Venant torsion, the associated shear stresses change sign and vary linearly across the wall thickness for open sections and thus can be considered to have no effect on local buckling [70]. Therefore, the cross-section St. Venant torsion resistance $T_{\mathrm{St,Rk}}$ of all open-sections can be approximated by the plastic St. Venant section resistance [70], which can be expressed by

Eq. (22) for I-sections, as given in [71], or can be approximated by Eq. (23), as recommended in [70], where τ_y is the shear yield stress which is equal to $f_y/\sqrt{3}$ and h, b, t_f and t_w are the overall depth, breadth, flange thickness and web thickness of the I-section, as shown in Fig. 4.

$$T_{St,Rk} = \tau_y \left[bt_f^2 \left(1 - \frac{t_f}{3b} \right) + \frac{(h - 2t_f)t_w^2}{2} + \frac{t_w^3}{6} \right] \tag{22}$$

$$T_{St,Rk} \approx \tau_y \left[bt_f^2 + \frac{(h - 2t_f)t_w^2}{2} \right] \tag{23}$$

For the case of warping torsion, the cross-section warping torsion resistance $T_{w,Rk}$ is taken as elastic warping torsion resistance $T_{w,el}$ in accordance with [72] in this study. As shown in Fig. 4, the shear force due to warping V_w can be approximated by resolving the warping torsion T_w into an equivalent force couple acting within the flanges $V_w = T_w/(h\text{-}t_f)$ [73]. By elastic analysis, the shear stress at the centre of the flange can be approximated by Eq. (24) [72].

$$\tau_w = \frac{1.5V_w}{bt_f} \tag{24}$$

Hence, the warping torsion resistance $T_{w,Rk}$ of an I-section, taken as $T_{w,el}$, can be determined as given by Eq. (25).

$$T_{w,Rk} = \tau_y bt_f (h - t_f)/1.5 \tag{25}$$

Note that the plastic warping resistance for I-sections is simply given by $T_{w,pl} = \tau_y bt_f(h\text{-}t_f)$.

6.1.2 Interaction of shear and torsion

According to prEN 1993-1-1 [15], for a cross-section subjected to combined torsion and shear, the plastic cross-section shear resistance should be reduced considering the adverse influence of shear stresses due to torsion. An expression for the reduced plastic vertical shear resistance $V_{pl,y,T}$ of I-sections in the presence of St. Venant torsion $T_{St,Ed}$ was developed in [74], as given by Eq. (26). This expression considers the interaction between the shear stresses due to vertical shear force $\tau_{y,Ed}$, which are uniformly distributed through the web thickness, and the shear

stresses due to St. Venant torsion $\tau_{\mathrm{St,Ed}}$, which vary linearly through the web thickness, as shown in Table 3, and forms the basis of the shear-torsion interaction formula given in prEN 1993-1-1 [15].

$$\text{For I-section, } V_{\mathrm{pl,y,T}} = \sqrt{1-\frac{T_{\mathrm{St,Ed}}}{T_{\mathrm{St,Rk}}}}V_{\mathrm{pl,y}} \tag{26}$$

Considering the different shear stress distributions through web thicknesses, as shown in Table 3, the equivalent expressions [74] for the determination of the reduced shear resistances of channels and square or rectangular hollow sections (SHS/RHS) subjected to combined torsion and shear were also set out in [74], as given by Eqs. (27) and (28).

$$\text{For channel section, } V_{\mathrm{pl,y,T}} = \left(\sqrt{1-\frac{T_{\mathrm{St,Ed}}}{T_{\mathrm{St,Rk}}}} - \frac{T_{\mathrm{w,Ed}}}{T_{\mathrm{w,Rk}}}\right)V_{\mathrm{pl,y}} \tag{27}$$

$$\text{For SHS/RHS, } V_{\mathrm{pl,y,T}} = \left(1-\frac{T_{\mathrm{St,Ed}}}{T_{\mathrm{St,Rk}}}\right)V_{\mathrm{pl,y}} \tag{28}$$

Clearly the ratio of the applied shear force to cross-section shear resistance (i.e. $V_{\mathrm{y,Ed}}/V_{\mathrm{pl,y,T}}$) has to be less than or equal to 1.0. In this study, the coefficients η_{y} and η_{z} are used to represent the utilisation of a cross-section under combined shear and torsion for shear forces acting through the cross-section depth (major axis bending cases) and the cross-section width (minor axis bending cases), respectively. The proposed expressions for the determination of η_{y} and η_{z} are provided in Table 4 for different cross-sections. The expressions for the determination of η_{y} in the cases where shear forces act through the cross-section depths were developed considering the shear stress distribution through the web thickness and using Eqs. (26)-(28). Similarly, to determine η_{z} for the cases where shear forces act through the cross-section widths, the interaction of the shear stresses due to lateral shear force $\tau_{\mathrm{z,Ed}}$, St. Venant torsion $\tau_{\mathrm{St,Ed}}$ and warping torsion $\tau_{\mathrm{w,Ed}}$ arising in the flanges, as presented in Table 3, was considered. Note that in Table 4, $V_{\mathrm{y,Ed}}$ and $V_{\mathrm{z,Ed}}$ are the vertical and lateral applied shear force respectively; $V_{\mathrm{y,Rk}}$ and

$V_{z,Rk}$ are the vertical and lateral cross-section shear resistances, taken as the plastic cross-section shear resistances $V_{pl,y}$ and $V_{pl,z}$ equal to $A_v\tau_y$, where A_v is the shear area determined according to prEN 1993-1-1 [15], and $T_{St,Rk}$ and $T_{w,Rk}$ are the cross-section St. Venant torsion and warping torsion resistances, respectively. $T_{St,Rk}$ can be determined using Eq. (23) for I-sections and channel sections and determined as $T_{St,Rk} = 2tA_0\tau_y$ for SHS/RHS, where t and A_0 are the section thickness and area enclosed by the mean perimeter [73], respectively; $T_{w,Rk}$ can be determined using Eq. (25) for I-sections and determined as $T_{w,Rk} = T_{w,el} = t_f I_w \tau_y / S_w$ for channel sections, where t_f, I_w and S_w are the flange thickness, cross-section warping constant and warping statical moment [75], respectively [73]. In the application of the proposed design method, shear checks for cross-sections should be performed to assess that Eq. (29) is satisfied.

$$T_{St,Ed}/T_{St,Rk} \leq 1.0,\ \eta_y \leq 1.0 \text{ and } \eta_z \leq 1.0 \tag{29}$$

Note that for cross-sections subjected to shear and/or torsion in which the web slenderness $\bar{\lambda}_w$ exceeds $0.83/\eta$, where $\eta = 1.2$ is the shear area factor [60], shear buckling should be accounted for in the determination of the cross-section shear resistances $V_{y,Rk}$ and $V_{z,Rk}$ and the warping torsion resistance $T_{w,Rk}$ according to [60].

6.1.3 Reduced CSM strain limits for the consideration of shear effects

Similar to the approach adopted in Section 5.2, the use of reduced CSM strain limits $\varepsilon_{csm,V}$ to take account of the interaction between bending, shear and torsion is recommended in the application of the proposed method, as given by:

$$\varepsilon_{csm,V} = \varepsilon_{csm} - \rho_y(\varepsilon_{csm} - \mu_{y,fl}\varepsilon_y) - \rho_z(\varepsilon_{csm} - \mu_{z,w}\varepsilon_y) \tag{30}$$

where ρ_y and ρ_z are the reduction factors ranging from 0 to 1.0 to allow for the influence of high vertical shear (including that resulting from torsion) and high lateral shear (including that resulting from torsion) on the ultimate cross-section resistance, and $\mu_{y,fl}$ and $\mu_{z,w}$ are given by:

$$\mu_{\mathrm{y,fl}} = \frac{M_{\mathrm{fl}}}{M_{\mathrm{el,y}}} \tag{31}$$

$$\mu_{\mathrm{z,w}} = \frac{M_{\mathrm{w}}}{M_{\mathrm{el,z}}}. \tag{32}$$

In Eqs. (31) and (32), $\mu_{\mathrm{y,fl}}$ is the ratio of the cross-section major axis bending moment resistance M_{fl} considering the flanges alone (i.e. neglecting the presence of the web) to the elastic major axis bending resistance of the full cross-section $M_{\mathrm{el,y}}$ (i.e. $M_{\mathrm{fl}}/M_{\mathrm{el,y}}$) and $\mu_{\mathrm{z,w}}$ is the ratio of the cross-section minor axis bending moment resistance determined neglecting the presence of the flanges M_{w} to the elastic minor axis bending resistance of the full cross-section $M_{\mathrm{el,z}}$ (i.e. $M_{\mathrm{w}}/M_{\mathrm{el,z}}$); these ratios are used to approximate the effectiveness of a cross-section in bending when the shear area (i.e. the web for major axis bending and the flanges for minor axis bending) is fully utilised in shear. M_{fl} can be calculated using Eq. (33); M_{w} (and hence $\mu_{\mathrm{z,w}}$) can be conservatively taken equal to 0 for I-sections, due to the insignificant contribution of the web to the cross-section minor axis bending resistance.

$$M_{\mathrm{fl}} = bt_{\mathrm{f}}(h - t_{\mathrm{f}})f_{\mathrm{y}} \tag{33}$$

Hence, for I-sections, the expression for calculating the reduced CSM strain limits $\varepsilon_{\mathrm{csm,V}}$ can be simplified to Eq. (34).

$$\text{For I-sections,}\quad \varepsilon_{\mathrm{csm,V}} = \varepsilon_{\mathrm{csm}} - \rho_{\mathrm{y}}(\varepsilon_{\mathrm{csm}} - \mu_{\mathrm{y,fl}}\varepsilon_{\mathrm{y}}) - \rho_{\mathrm{z}}\varepsilon_{\mathrm{csm}} \tag{34}$$

prEN 1993-1-1 [15] accounts for the interaction between vertical shear effects (arising from shear force and torsion) and major axis bending by reducing the cross-section bending capacities for the cases where the ratio of the applied shear force to the plastic cross-section shear resistance exceeds 0.5. The reduced bending moment capacity is determined using a reduced yield strength $(1 - \rho_{\mathrm{y,EC3}})f_{\mathrm{y}}$ for the shear area, where the reduction factor $\rho_{\mathrm{y,EC3}}$ is given by Eq. (35).

$$\rho_{\mathrm{y,EC3}} = \begin{cases} 0 & \text{for } \dfrac{V_{\mathrm{y,Ed}}}{V_{\mathrm{pl,y,T}}} \le 0.5 \\ \left(\dfrac{2V_{\mathrm{y,Ed}}}{V_{\mathrm{pl,y,T}}} - 1\right)^2 & \text{for } 0.5 < \dfrac{V_{\mathrm{y,Ed}}}{V_{\mathrm{pl,y,T}}} \le 1.0 \end{cases} \tag{35}$$

In this study, the reduction factor ρ_{y} used in Eqs. (30) and (34) adopts a similar format, as given by Eq. (36), where the major axis shear-torsion interaction factor η_{y} is presented in Table 4 and illustrated in Section 6.1.2.

$$\rho_{\mathrm{y}} = \begin{cases} 0 & \text{for } \eta_{\mathrm{y}} \le 0.5 \\ \left(2\eta_{\mathrm{y}} - 1\right)^2 & \text{for } 0.5 < \eta_{\mathrm{y}} \le 1.0 \end{cases} \tag{36}$$

In prEN 1993-1-1 [15], for members subjected to significant shear forces through their cross-section widths, the yield strength of the shear area is reduced by $\rho_{\mathrm{z,EC3}}$, which is determined using Eq. (37) for I-sections and channels and Eq. (38) for SHS/RHS. Note that the von Mises yield criterion was considered in the development of the expression for I-sections and channel sections [76] and that the reduction to the yield strength is applied when the ratio of the applied shear force $V_{\mathrm{z,Ed}}$ to the plastic shear resistance ($V_{\mathrm{z,Ed}}/V_{\mathrm{pl,z}}$) is higher than 0.25.

$$\text{For I-sections and channel sections, } \rho_{\mathrm{z,EC3}} = \begin{cases} 0 & \text{for } \dfrac{V_{\mathrm{z,Ed}}}{V_{\mathrm{pl,z}}} \le 0.25 \\ 1 - \sqrt{1 - \left(\dfrac{V_{\mathrm{z,Ed}}}{V_{\mathrm{pl,z}}}\right)^2} & \text{for } 0.25 < \dfrac{V_{\mathrm{z,Ed}}}{V_{\mathrm{pl,z}}} < 1.0 \\ 1 & \text{for } \dfrac{V_{\mathrm{z,Ed}}}{V_{\mathrm{pl,z}}} = 1.0 \end{cases} \tag{37}$$

$$\text{For SHS/RHS, } \rho_{\mathrm{z,EC3}} = \begin{cases} 0 & \text{for } \dfrac{V_{\mathrm{z,Ed}}}{V_{\mathrm{pl,z}}} \le 0.5 \\ \left(\dfrac{2V_{\mathrm{z,Ed}}}{V_{\mathrm{pl,z}}} - 1\right)^2 & \text{for } 0.5 < \dfrac{V_{\mathrm{z,Ed}}}{V_{\mathrm{pl,z}}} \le 1.0 \end{cases} \tag{38}$$

Following the format adopted in prEN1993-1-1 [15], in this study, for I-sections and channel sections, Eq. (39) is recommended for the determination of the reduction factor ρ_{z} used in Eqs. (30) or (34), as given by

$$\text{For I-sections and channel sections, } \rho_z = \begin{cases} 0 & \text{for } \eta_z \le 0.25 \\ 1-\sqrt{1-\eta_z^2} & \text{for } 0.25<\eta_z<1.0 \\ 1 & \text{for } \eta_z = 1.0 \end{cases} \tag{39}$$

For SHS/RHS, the reduction factor ρ_z can be determined using Eq. (40).

$$\text{For SHS/RHS, } \rho_z = \begin{cases} 0 & \text{for } \eta_z \le 0.5 \\ (2\eta_z - 1)^2 & \text{for } 0.5<\eta_z \le 1.0 \end{cases} \tag{40}$$

In both Eqs. (39) and (40), the minor axis shear-torsion interaction factor η_z should be determined from Table 4.

6.2 Accuracy of proposed design approach for laterally-restrained beams

In this subsection, the accuracy of the proposed approach for the design of laterally-restrained steel beams under in-plane bending and shear without the presence of torsion is investigated. Fig. 18 (a) shows the reducing CSM strain limit $\varepsilon_{csm,V}/\varepsilon_y$ determined using Eq. (34), with increasing $V_{y,Ed}/V_{pl,y}$ ratios for steel beams made of grade S355 steel with an HEB 100 cross-section and subjected to in-plane 3-point major axis bending, while Fig. 18 (b) illustrates the ultimate capacities of the beams with different normalised member lengths $L/L_{b,cs}$ obtained from the shell FE models $M_{u,shell}$ and the proposed design method $M_{u,prop}$ using the unreduced ε_{csm} and reduced $\varepsilon_{csm,V}$ CSM strain limits plus the shear check. It can be seen from the figure that, for beams with high shear forces, the application of the proposed design method without the consideration of the shear effects may lead to unconservative member capacity predictions; on the other hand, employing the reduced strain limits and shear checks shift these unconservative predictions to the safe side.

Similar conclusions can also be drawn from the results of a number of I-section members (including 10 IPE, 10 HEB and 10 HEA profiles with 10 varied member lengths) subjected to 3-point major axis bending shown in Fig. 19. Fig. 19 (a) shows the normalised moment-shear interaction obtained from shell FE models and the proposed design method using the unreduced

ε_{csm} and reduced $\varepsilon_{csm,V}$ CSM strain limits plus the shear check, where V_u is the ultimate shear capacity obtained from different design methods. It can be seen from the figure that in bending-dominated cases, the beneficial effects from the local moment gradients outweigh the negative influence from shear effects; thus, with increasing shear forces, increases in the bending moment capacities can be observed [31]. On the other hand, in the shear-dominated cases, reducing the CSM strain limits considering high shear effects and performing shear checks moves unsafe predictions that can be observed without any shear checks to the safe side; this also can be seen from Fig. 19 (b), which shows a comparison between the member capacities obtained from the proposed method using ε_{csm} and $\varepsilon_{csm,V}$ plus the shear check, normalised by the corresponding shell FE results, versus the value of η_y at the attainment of the peak load factor or ε_{csm}.

Fig. 20 shows comparisons between member capacity predictions obtained using the proposed design method $M_{u,prop}$ with unreduced CSM limits ε_{csm} and reduced CSM limits $\varepsilon_{csm,V}$ plus the shear check, which are normalised by shell FE results for I-section members (including 10 IPE, 10 HEB and 10 HEA profiles with 4 different member lengths) subjected to 3-point minor axis bending and 38 SHS/RHS members subjected to 3-point major and minor axis bending, versus the value of η_y or η_z at the attainment of the peak load factor or ε_{csm}. As can be seen from the figure, the application of the proposed design method with $\varepsilon_{csm,V}$ provides safe and accurate member capacity predictions.

6.3 Accuracy of proposed design approach for laterally-unrestrained beams

In this subsection, the accuracy of the proposed design approach for beams subjected to bending alone and susceptible to LTB, where torsion is induced as a second-order effect, is investigated. Fig. 21 shows a comparison between the ultimate resistance predictions obtained from the proposed design method $M_{u,prop}$ using the reduced strain limit $\varepsilon_{csm,V}$ determined from Eq. (34), which considers the influence of shear stresses resulting from applied shear forces

and torsion (second-order torsion in this case), and using the reduced strain limit proposed in [21] $\rho_{csm}\varepsilon_{csm}$ (see Section 5.2), which only considers the influence of shear stresses from applied shear for all studied beams subjected to non-uniform bending. It can be seen from the figure that the two approaches lead to very close predictions (differences are within 5%) of member capacities. Since the consideration of shear effects due to second-order torsion generally has only a slight influence on the strength predictions of steel beams subjected to bending alone, the formula (Eq. (18)) presented in Section 5.2, which only considers the influence of shear stresses from applied shear forces, can also be used in these cases as it provides accurate and safe member capacity predictions.

6.4 Accuracy of proposed design approach for members subjected to torsion

In this subsection, the accuracy of the proposed design method is assessed for steel beams subjected to torsion (directly applied rather than as a consequence of instability), considering different cross-sections, member lengths and loading conditions.

In the assessment of the proposed design approach for steel beams with I-sections and subjected to torsion, (i) 200 steel beams subjected to concentrated lateral load $2P$ (generating an internal shear force V_z) and concentrated torsion $2T$ at the midspan with the ratio of $0.5V_zL/T$ = 2, 5, 10 and 20, (ii) 200 steel beams subjected to concentrated vertical load $2P$ (generating an internal shear force V_y) and concentrated torsion $2T$ at the midspan with the ratio of $(T/T_{St,Rk})/(0.5V_yL/M_{pl,y})$ = 0.4, 1, 4, 7 and 10, (iii) 200 steel beams subjected to uniform bending M and concentrated torsion $2T$ at the midspan with the ratio of $(T/T_{St,Rk})/(M/M_{pl,y})$ = 0.4, 1, 4, 7 and 10 and (iv) 180 extreme cases where steel beams were subjected to only concentrated torsion moments $2T$ at the midspan were considered.

In Fig. 22, the ultimate capacities obtained from the proposed design method using unreduced ε_{csm} and reduced $\varepsilon_{csm,V}$ strain limits as well as shear checks versus the maximum shear-torsion

interaction factors $\eta_{y,max}$ or $\eta_{z,max}$ along the member lengths at failure due to attainment of the peak loads or strain limits ε_{csm} without considering shear effects are illustrated. Note that in the figure, the ultimate strengths determined through the proposed design method are normalised by the benchmark shell FE results. As can be seen from Fig. 22, the consideration of shear effects due to torsion now has a significant influence on the strength predictions of the considered members subjected to torsion. Particularly, for the case of members under pure torsion, the neglect of the shear effects from torsion in the application of the proposed method can lead to unsafe torsion resistance predictions $T_{u,prop}$, where the predictions can be up to 85% higher than the torsion resistances obtained from the shell FE models $T_{u,shell}$. On the other hand, as can be seen from Fig. 22, if the shear check and the reduced strain limits $\varepsilon_{csm,V}$, which take account of the shear effect from torsion are employed, the great majority of the unsafe predictions shift to the safe side with only few predictions remaining slightly on the unsafe, but with acceptable margins (within 7%).

In addition to I-section steel members, 70 SHS/RHS members subjected to combined concentrated (vertical or lateral) load $2P$, generating a shear force V, and concentrated torsion $2T$ at the midspan and 15 SHS/RHS members subjected to pure torsion were also studied; the results are presented in Fig. 23. Similar to the conclusions drawn from the results for I-section members, Fig. 23 shows that it is necessary to consider the influence of high shear arising from the application of torsion and employ the reduced strain limits $\varepsilon_{csm,V}$ plus the shear check in the application of the proposed design method, to achieve accurate and safe ultimate capacity predictions.

It should be noted that, in the application of the proposed design method, for members subjected to combined major or minor axis bending and torsion, the elastic local buckling stress $\sigma_{cr,cs}$ used to determine the cross-section slenderness $\bar{\lambda}_p$ and hence the CSM strain limit were calculated considering the normal stress distributions arising from major or minor axis bending

moments. For the pure torsion cases, since the only normal stresses induced in the member are warping torsion normal stresses, which are distributed within each flange in a similar fashion to that when the cross-section is subjected to minor axis bending, as shown in Fig. 4, the elastic local buckling stress $\sigma_{cr,cs}$ was calculated assuming that the cross-section is under minor axis bending. For members under torsion, local buckling half-wavelengths $L_{b,cs}$ used to average strains were conservatively taken as the lower value of the local buckling half-wavelengths of the single web and single flange plates with fixed boundary conditions, which is the lower bound envelope of the local buckling half-wavelength of full cross-sections [54].

7. WORKED EXAMPLE

A worked example is presented in this section to illustrate the implementation of the proposed design method. The example considers a beam made of grade S355 steel (f_y = 355 MPa, f_u = 510 MPa, reduced value of E = 200000 MPa and ν = 0.3) with a hot-rolled HEA 260 cross-section and a length of 13000 mm (i.e. L = 13000 mm); the considered beam is subjected to major axis bending moments $M_{y,Ed}$ = 120 kNm applied at the two ends, as shown in Fig. 24.

The proposed design approach requires a GMNIA of the member using beam finite elements to be performed, as described in Section 3.2. As shown in Fig. 24 (a), which summarises the application of the proposed method to the considered beam, the quad-linear material model described in Section 3.1, converted into a true stress-strain relationship was adopted; 91 B31OS beam elements were used to model the member; the equivalent imperfection was modelled through the scaling of the first LTB eigenmode with an amplitude of $e_{0,LT} = \alpha_z L/150$ = 42.47 mm, where α_z is the imperfection factor taken as 0.49 for the considered cross-section in accordance with the recommendations made in [46]. After performing GMNIA, the design resistance factor of the beam can be obtained following the steps set out below.

I. Calculation of full cross-section elastic local buckling stress $\sigma_{cr,cs}$

The expressions developed by Gardner et al. [33] are used to determine the elastic local buckling stress of the full cross-section $\sigma_{\mathrm{cr,cs}}$. The plate buckling coefficients for the isolated flange under uniform compression with simply-supported and fixed boundary conditions are equal to $k_{\mathrm{f}}^{\mathrm{SS}} = 0.43$ and $k_{\mathrm{f}}^{\mathrm{F}} = 1.25$, respectively. Likewise, the plate buckling coefficients for the isolated web under pure bending with simply-supported and fixed boundary conditions are equal to $k_{\mathrm{w}}^{\mathrm{SS}} = 23.9$ and $k_{\mathrm{w}}^{\mathrm{F}} = 39.6$, respectively. Using these buckling coefficients, the corresponding elastic buckling stresses of the isolated flange and web are determined as $\sigma_{\mathrm{cr,f}}^{\mathrm{SS}}$ = 718.6 MPa, $\sigma_{\mathrm{cr,f}}^{\mathrm{F}}$ = 2089.1 MPa, $\sigma_{\mathrm{cr,w}}^{\mathrm{SS}}$ = 4308.2 MPa, $\sigma_{\mathrm{cr,w}}^{\mathrm{F}}$ = 7138.3 MPa. The lower and upper bounds to the full cross-section local buckling stress are thus equal to $\sigma_{\mathrm{cr,p}}^{\mathrm{SS}}$ = 718.6 MPa and $\sigma_{\mathrm{cr,p}}^{\mathrm{F}}$ = 2089.1 MPa. The interaction coefficient ζ, to account for the effect of element interaction [33], is given by:

$$\zeta = \max(0.15\frac{t_{\mathrm{f}}}{t_{\mathrm{w}}}\phi,\ \frac{t_{\mathrm{w}}}{t_{\mathrm{f}}}(0.4 - 0.25\phi)) = 0.215 \tag{41}$$

where $\phi = \sigma_{\mathrm{cr,f}}^{\mathrm{SS}} / \sigma_{\mathrm{cr,w}}^{\mathrm{SS}} = 0.167$. The full cross-section elastic local buckling stress $\sigma_{\mathrm{cr,cs}}$ is determined as

$$\sigma_{\mathrm{cr,cs}} = \sigma_{\mathrm{cr,p}}^{\mathrm{SS}} + \zeta\left(\sigma_{\mathrm{cr,p}}^{\mathrm{F}} - \sigma_{\mathrm{cr,p}}^{\mathrm{SS}}\right) = 1013 \text{ MPa.} \tag{42}$$

Note that the finite strip analysis software *CUFSM* [42] gives a full cross-section elastic local buckling stress of 1001 MPa.

II. Calculation of cross-section slenderness $\bar{\lambda}_{\mathrm{p}}$

Using Eq. (10), the cross-section slenderness is determined as $\bar{\lambda}_{\mathrm{p}} = \sqrt{f_{\mathrm{y}} / \sigma_{\mathrm{cr,cs}}}$ = 0.59.

III. Calculation of CSM strain limit $\varepsilon_{\mathrm{csm}}$

Based on the cross-section slenderness, the CSM strain limit can be calculated using Eqs. (8) and (9). For this example, with $\bar{\lambda}_p$= 0.59, the CSM strain limit $\varepsilon_{csm}/\varepsilon_y$ is equal to 1.65.

IV. Calculation of elastic local buckling half-wavelength $L_{b,cs}$

The expressions developed by Fieber et al. [54] are used to calculate the elastic local buckling half-wavelength $L_{b,cs}$ of the beam. The lower and upper bounds to the local buckling half-wavelength are given by $L_{b,p}^{F} = 214.5\text{ mm}$ and $L_{b,p}^{SS} = 489\text{ mm}$. Using these values, the elastic local buckling half-wavelength of the full cross-section is determined as:

$$L_{b,cs} = L_{b,p}^{SS} - \zeta\left(L_{b,p}^{SS} - L_{b,p}^{F}\right) = 430\text{ mm}. \tag{43}$$

Note that the finite strip analysis software *CUFSM* [42] provides an elastic local buckling half-wavelength of 450 mm. Based on the calculated local buckling half-wavelength $L_{b,cs}$ = 430 mm, within which 3 beam elements fully lie, the average maximum compressive normal strain for each finite element $\varepsilon_{Ed,av,m}$ along the length of the considered beam can be determined.

V. Determination of failure mode and characteristic resistance factor

The load increments at the attainment of the peak load factor and CSM strain limit in the GMNIA can now be determined. Fig. 24 (b) shows the load factor α (i.e. $M/M_{y,Ed}$) versus average maximum compressive strain at the critical location (i.e. the midspan in this case) path of the considered beam. It can be seen that in this case, the average strain at the midspan reaches the CSM strain limit prior to the attainment of the peak load factor. Thus, the member is deemed to fail at the load factor α_{csm} = 1.129, and the characteristic resistance factor α_{Rk} is equal to 1.129 (i.e. α_{Rk} = 1.129). Note that at the failure moment, the shear-torsion factors η_y = 0 and η_z = 0.010 are very small; thus, the shear due to torsion is negligible, and there is no need to reduce the strain limits.

VI. Determination of design resistance factor

As mentioned in Section 3.3, the application of the partial safety factor (γ_{M1} = 1.0 for member stability calculations) to the characteristic resistance factor is necessary to obtain the design resistance factor, as given by Eq. (17). Hence, in this worked example, the design resistance factor of the member is given by:

$$\alpha_{Rd} = \alpha_{Rk} / \gamma_{M1} = 1.129 / 1.0 = 1.129 > 1.0. \qquad \therefore \text{Pass} \tag{44}$$

The beam is thus able to withstand the applied forces and its design bending moment resistance is equal to $M_{Rd} = \alpha_{Rd} M_{y,Ed}$ = 135.48 kNm, according to the proposed method. On the other hand, using the lateral-torsional buckling design expressions provided in prEN 1993-1-1 [15], the design bending moment resistance of the beam is calculated as 105.46 kNm, which is equal to 88% of the applied bending moment, indicating that the beam is not able to withstand the applied bending moment. It is worth noting that the benchmark shell finite element model of the considered beam provides a resistance factor of $\alpha_{u,shell}$ = 1.134 (i.e. $M_{u,shell}$ = 136.03 kNm), which is very close to the ultimate resistance factor obtained through the proposed design method, but is lower than the bending resistance corresponding to the peak load factor α_{peak} = 1.281, i.e. the resistance that would be obtained if cross-section failure, as defined by the CSM strain limit, were to be ignored.

8. CONCLUSIONS

A new method for the design of steel beams against lateral-torsional buckling (LTB) performed by advanced inelastic analysis using beam finite elements with CSM strain limits has been put forward in this paper. The proposed method is performed by carrying out a Geometrically and Materially Nonlinear Analysis with Imperfections (GMNIA) of a steel member using beam finite elements and defining the ultimate resistance as (i) the peak load factor α_{peak} after which the load-deformation curve descends or (ii) the load factor that corresponds to the attainment of the CSM strain limit α_{csm}, whichever occurs first. Shell finite element models able to

replicate the LTB response of steel beams were created and validated against experimental results from the literature. Using the validated shell FE models, the accuracy of the proposed design method was extensively verified for 300 steel I-section beams subjected to uniform bending and 1200 steel beams subjected to non-uniform bending, considering a range of European cross-section profiles, member slendernesses and bending moment gradients. It was shown that the proposed method consistently provides more accurate ultimate strength predictions relative to the traditional beam design method provided in prEN 1993-1-1 [15]. The high accuracy of the proposed design method derives from (i) recognising the interaction between cross-section elements during local buckling through the use of the cross-section slendernesses in the determination of the CSM strain limits, (ii) allowing for strain hardening, (iii) exploiting of partial plastification in Class 3 cross-sections and (iv) considering the beneficial effects of local strain gradients along the member lengths. The proposed method also removes the need for cross-section classification, individual member buckling checks and the calculation of effective lengths in the determination of the ultimate strengths of members, thereby significantly streamlining the structural steel design process and providing the ultimate resistances and failure modes of steel members and systems directly. In addition to steel beams under bending alone, the proposed method was also developed for and applied to steel I-section members subjected to (i) bending and shear, (ii) bending and torsion, (iii) bending, shear and torsion and (iv) pure torsion, where the safety and accuracy of method were illustrated. For pure bending cases, the consideration of shear effects due to second-order torsion had only a slight influence on strength predictions, and thus can be eliminated in the proposed design method, while for members subjected to primary torsion actions, shear effects due to torsion have to be taken into account. Provisions for considering shear-torsion effects for SHS/RHS and channel sections were also presented in this study. The research presented herein extends, for the first time, the scope of the method of design by GMNIA with CSM strain limits from

in-plane to out-of-plane stability problems, enabling its general applicability to three-dimensional structural systems.

ACKNOWLEDGEMENTS

The financial support provided by the China Scholarship Council (CSC) and Imperial College London for the first author is gratefully acknowledged.

REFERENCES

[1] T.V. Galambos, M.K. Ravindra, Load and resistance factor design criteria for steel beams, Structural Division, Civil and Environmental Engineering Department, Washington University, 1974.

[2] ECCS, Manual on stability of steel structures, Tech. Rep.; No. 22, Technical Committee 8 (TC 8) of European Convention for Constructional Steelwork (ECCS). 1976.

[3] D.A. Nethercot, N.S. Trahair, Inelastic lateral buckling of determinate beams, J. Struct. Div. ASCE 102 (4) (1976) 701-717.

[4] J.A. Yura, M.K. Ravindra, T.V. Galambos, The bending resistance of steel beams, J. Struct. Div. ASCE 104 (9) (1978) 1355-1370.

[5] B.G. Neal, Lateral instability of yielded mild steel beams of rectangular cross-section, Philos. Trans. R. Soc. London. Ser. A, Math. Phys. Sci. 242 (1950) 197-242.

[6] W.H. Wittrick, Lateral instability of rectangular beams of strain hardening material under uniform bending, J. Aeron. Sci. 19 (12) (1952) 835-843.

[7] N.S. Trahair, S. Kitipornchai, Buckling of inelastic I-beams under uniform moment, J. Struct. Div. ASCE 98 (11) (1972) 2551-2566.

[8] N.S. Trahair, G.J. Hancock, Steel member strength by inelastic lateral buckling, J. Struct. Eng. ASCE 130 (1) (2003) 64-69.

[9] N.S. Trahair, Steel cantilever strength by inelastic lateral buckling, J. Constr. Steel Res. 66 (2010) 993-999.

[10] N.S. Trahair, Inelastic buckling design of monosymmetric I-beams, Eng. Struct. 34 (2012) 564-571.

[11] M. Kucukler, L. Gardner, L. Macorini, Lateral-torsional buckling assessment of steel beams through a stiffness reduction method, J. Constr. Steel Res. 109 (2015) 87-100.

[12] M. Kucukler, L. Gardner, L. Macorini, Flexural-torsional buckling assessment of steel beam-columns through a stiffness reduction method, Eng. Struct. 101 (2015) 662-676.

[13] M. Kucukler, L. Gardner, Design of web-tapered steel beams against lateral-torsional buckling through a stiffness reduction method, Eng. Struct. 190 (2019) 246-261.

[14] EN 1993-1-1. Eurocode 3: Design of steel structures - Part 1-1: General rules and rules for buildings. European Committee for Standardization, Brussels, 2005.

[15] prEN 1993-1-1. Eurocode 3: Design of steel structures - Part 1-1: General rules and rules for buildings. 2019.

[16] AISC 360-16, Specifications for Structural Steel Buildings, American Institute of Steel Construction (AISC), Chicago, 2016.

[17] AS 4100, Standards Australia, AS 4100 Steel Structures, Australian Building Codes Board, Sydney, 1998.

[18] R. Ofner, Traglast von Staben aus Stahl bei Druck und Biegung, PhD thesis, Institut fur Stahlbau, Holzbau und Flachentragwerke, TU Graz, Heft 9, 1997.

[19] G. Salzgeber, Nichtlineare Berechnung von raumlichen Stabtragwerken aus Stahl, Dissertation, Institut fur Stahlbau, Holzbau und Flachentragwerke, TU Graz, Heft 10, 2000.

[20] J. Lindner, S. Heyde, Evaluation of interaction formulae at Level 1 approach with regard to ultimate load calculations and test results—flexural buckling and lateral torsional buckling, Report 2144E, TU Berlin, ECCS Report No. TC8-2001-017, 2001.

[21] P. Kaim, Spatial buckling behaviour of steel members under bending and axial compression, PhD thesis, Institute for Steel, Timber and Shell Structures, TU Graz, Heft 12, 2004.

[22] R. Greiner, J. Lindner, Interaction formulae for members subjected to bending and axial compression in Eurocode 3 – The Method 2 approach, J. Constr. Steel Res., 62 (2006) 757-770.

[23] J.P. Jaspart, Ch. Briquet, R. Maquoi, Comparative study of beam-column interaction formulae, Proc. of the Annual Meeting of the Structural Stability Research Council, Milwaukee, 1993, 369-380.

[24] M. Villette, N. Boissonnade, J.P. Muzeau, J.P. Jaspart, Development of a comprehensive formula for the design of beam-columns. Internal report, Baudin-Chateauneuf, LERMES-CUST, University of Liege, 2000.

[25] N. Boissonnade, J.P. Jaspart, J.P. Muzeau, M. Villette, Improvement of the interaction formulae for beam-columns in Eurocode 3, Computers and Structures. 80 (2002) 2375-2385.

[26] N. Boissonnade, J.P. Jaspart, J.P. Muzeau, M. Villette, New Interaction formulae for beam-columns in Eurocode 3: The French-Belgian approach, J. Constr. Steel Res. 60 (2004) 421-431.

[27] N. Boissonnade, R. Greiner R, J.P. Jaspart, J. Lindner, Rules for Member Stability in EN 1993-1-1: background documentation and design guidelines, No 119, ECCS European Convention for Constructional Steelwork, 2006.

[28] L. Gardner, The continuous strength method, Proc. Inst. Civ. Eng. Struct. Build. 161 (2008) 127-133.

[29] L. Gardner, X. Yun, A. Fieber, L. Macorini, Steel Design by Advanced Analysis: Material Modeling and Strain Limits, Engineering. 5 (2019) 243-249.

[30] A. Fieber, L. Gardner, L. Macorini, Structural steel design using second-order inelastic analysis with strain limits, J. Constr. Steel Res. 168 (2020) 105980.

[31] A. Fieber, L. Gardner, L. Macorini, Design of structural steel members by advanced inelastic analysis with strain limits, Eng. Struct. 199 (2019) 109624.

[32] F. Walport, L. Gardner, D.A. Nethercot, Design of structural stainless steel members by second order inelastic analysis with CSM strain limits, Thin-Walled Struct. 159 (2020) 107267.

[33] L. Gardner, A. Fieber, L. Macorini, Formulae for calculating elastic local buckling stresses of full structural cross-sections, Structures. 17 (2019) 2-20.

[34] C. Quan, M. Kucukler, L. Gardner, Design of web-tapered steel I-section members by second-order inelastic analysis with strain limits, Eng. Struct. 224 (2020) 111242.

[35] M. Ashraf, L. Gardner, D.A. Nethercot, Structural stainless steel design: Resistance based on deformation capacity, J. Struct. Eng. 134 (2008) 402-411.

[36] S. Afshan, L. Gardner, The continuous strength method for structural stainless steel design, Thin-Walled Struct. 68 (2013) 42-49.

[37] X. Yun, L. Gardner, N. Boissonnade, The continuous strength method for the design of hot-rolled steel cross-sections, Eng. Struct. 157 (2018) 179-191.

[38] X. Yun, L. Gardner, N. Boissonnade, Ultimate capacity of I-sections under combined loading - Part 2: Parametric studies and CSM design, J. Constr. Steel Res. 148 (2018) 265-274.

[39] M. Ashraf, B. Young, Design formulations for non-welded and welded aluminium columns using Continuous Strength Method, Eng. Struct. 33 (2011) 3197-3207.

[40] M.N. Su, B. Young, L. Gardner, Deformation-based design of aluminium alloy beams, Eng. Struct. 80 (2014) 339-349.

[41] M.N. Su, B. Young, L. Gardner, The continuous strength method for the design of aluminium alloy structural elements, Eng. Struct. 122 (2016) 338-348.

[42] Z. Li, B.W.Schafer, Buckling analysis of cold-formed steel members with general boundary conditions using CUFSM: Conventional and constrained finite strip methods. In Twentieth International Speciality Conference on Cold-Formed Steel Structures. Saint Louis, Missouri, USA, 2010.

[43] X. Yun, L. Gardner, Stress-strain curves for hot-rolled steels, J. Constr. Steel Res. 133 (2017) 36-46.

[44] ABAQUS. ABAQUS/standard user's manual. Version 6.17. Dassault Systemes Simulia Corp. USA; 2017.

[45] F. Walport, L. Gardner, D.A. Nethercot, Equivalent bow imperfections for use in design by second order inelastic analysis, Structures. 26 (2020) 670-685.

[46] C. Quan, F. Walport, L. Gardner, Equivalent imperfections for the out-of-plane stability design of steel beams by second-order inelastic analysis, submitted.

[47] G.C. Driscoll Jr., L.S. Beedle, The plastic behavior of structural members and frames, Weld. J. 36 (1957) 275-s.

[48] V. Gioncu, D. Petcu, Available rotation capacity of wide-flange beams and beam-columns Part 2. Experimental and numerical tests, J. Constr. Steel Res. 43 (1997) 219-244.

[49] M.G. Lay, T.V. Galambos, The inelastic behavior of beams under moment gradient. Fritz Engineering Laboratory Report No. 297.12, Lehigh University, 1964.

[50] X. Meng, L. Gardner, Cross-sectional behaviour of cold-formed high strength steel circular hollow sections, Thin-Walled Struct. 156 (2020) 106822.

[51] J. Wang, S. Afshan, M. Gkantou, M. Theofanous, C. Baniotopoulos, L. Gardner, Flexural behaviour of hot-finished high strength steel square and rectangular hollow sections, J. Constr. Steel Res. 121 (2016) 97-109.

[52] L. Gardner, N. Saari, F. Wang, Comparative experimental study of hot-rolled and cold-formed rectangular hollow sections, Thin-Walled Struct. 48 (7) (2010) 495-507.

[53] A. Fieber, Structural steel design using advanced analysis with strain limits, PhD thesis, Imperial College London, 2019.

[54] A. Fieber, L. Gardner, L. Macorini, Formulae for determining elastic local buckling half-wavelengths of structural steel cross-sections, J. Constr. Steel Res. 159 (2019) 493-506.

[55] M. Kucukler, L. Gardner, Design of laterally restrained web-tapered steel structures through a stiffness reduction method, J. Constr. Steel Res. 141 (2018) 63-76.

[56] Z. Xing, M. Kucukler, L. Gardner, Local buckling of stainless steel plates in fire, Thin-Walled Struct. 148 (2020) 106570.

[57] M. Kucukler, Z. Xing, L. Gardner, Behaviour and design of stainless steel I-section columns in fire, J. Constr. Steel Res. 165 (2020) 105890.

[58] M. Kucukler, Lateral instability of steel beams in fire: Behaviour, numerical modelling and design, J. Constr. Steel Res. 170 (2020) 106095.

[59] ECCS, Ultimate Limit State Calculation of Sway Frames with Rigid Joints, Tech. Rep.; No. 33, Technical Committee 8 (TC 8) of European Convention for Constructional Steelwork (ECCS). 1984.

[60] EN 1993-1-5. Eurocode 3: Design of steel structures Part 1-5: Plated structural elements. European Committee for Standardization, Brussels, 2006.

[61] G.B. dos Santos, L. Gardner, M. Kucukler, A method for the numerical derivation of plastic collapse loads, Thin-Walled Struct. 124 (2018) 258-277.

[62] P.F. Dux, S. Kitipornchai, Inelastic beam buckling experiments, J. Constr. Steel Res. 3 (1983) 3-9.

[63] H. Ozbasaran, R. Aydin, M. Dogan, An alternative design procedure for lateral-torsional buckling of cantilever I-beams, Thin-Walled Struct. 90 (2015) 235-242.

[64] A.L. Demirhan, H.E. Eroğlu, E.O. Mutlu, T. Yılmaz, Ö. Anil, Experimental and numerical evaluation of inelastic lateral-torsional buckling of I-section cantilevers, J. Constr. Steel Res. 168 (2020) 105991.

[65] L. Schaper, F. Jörg, R. Winkler, U. Kuhlmann, M. Knobloch, The simplified method of the equivalent compression flange: Development based on LTB tests and residual stress measurements, Steel Constr. 12 (2019) 264-277.

[66] A.R. Tusnin, M. Prokic, Selection of parameters for I-beam experimental model subjected to bending and torsion, Procedia Eng. 111 (2015) 789-796.

[67] A.R. Tusnin, M. Prokic, Experimental research of I-beams under bending and torsion actions, Mag. Civ. Eng. 53 (2015) 24-31.

[68] B.G. Estabrooks, G.Y. Grondin, Combined Bending and Torsion of Steel I-Shaped Beams, University of Alberta, (2008).

[69] J. Lindner, T. Glitsch, Vereinfachter Nachweis für I- und U-Träger beansprucht durch doppelte Biegung und Torsion, Stahlbau. 73 (2004) 704-715.

[70] N.S. Trahair, M.A. Bradford, D.A. Nethercot, L. Gardner, The behaviour and design of steel structures to EC3 (4th edn.), Spon Press, British. London (2007).

[71] Y.L. Pi, N.S. Trahair, Inelastic torsion of steel I-beams, J. Struct. Eng. 121 (1995) 609-620.

[72] P.A. Seaburg, C.J. Carter, Torsional Analysis of Structural Steel Members, AISC Steel Design Guide Series No.9, 2003.

[73] A.F. Hughes, D.C. Iles, A.S. Malik, SCI P385 Design of Steel Beams in Torsion, 2011.

[74] E. Mirambell, J. Bordallo, E. Real, Torsion and its interaction with other internal forces in EN 1993-1-1 – a new approach, Steel Constr. 9 (2016) 240-248.

[75] T.V. Galambos, Structural Members and Frames, Prentice-Hall, Englewood Cliffs, NJ, 1968.

[76] M. Knobloch, U. Kuhlmann, L. Lindner, F. Jörg, R. Winkler, Effect of shear forces on the bending moment resistance – Proposal of Amendments on prEN 1993-1-1:2018 CI.8.2.8, CEN/TC 250/SC 3/WG 1 N 272, 2019.

Graphical abstract

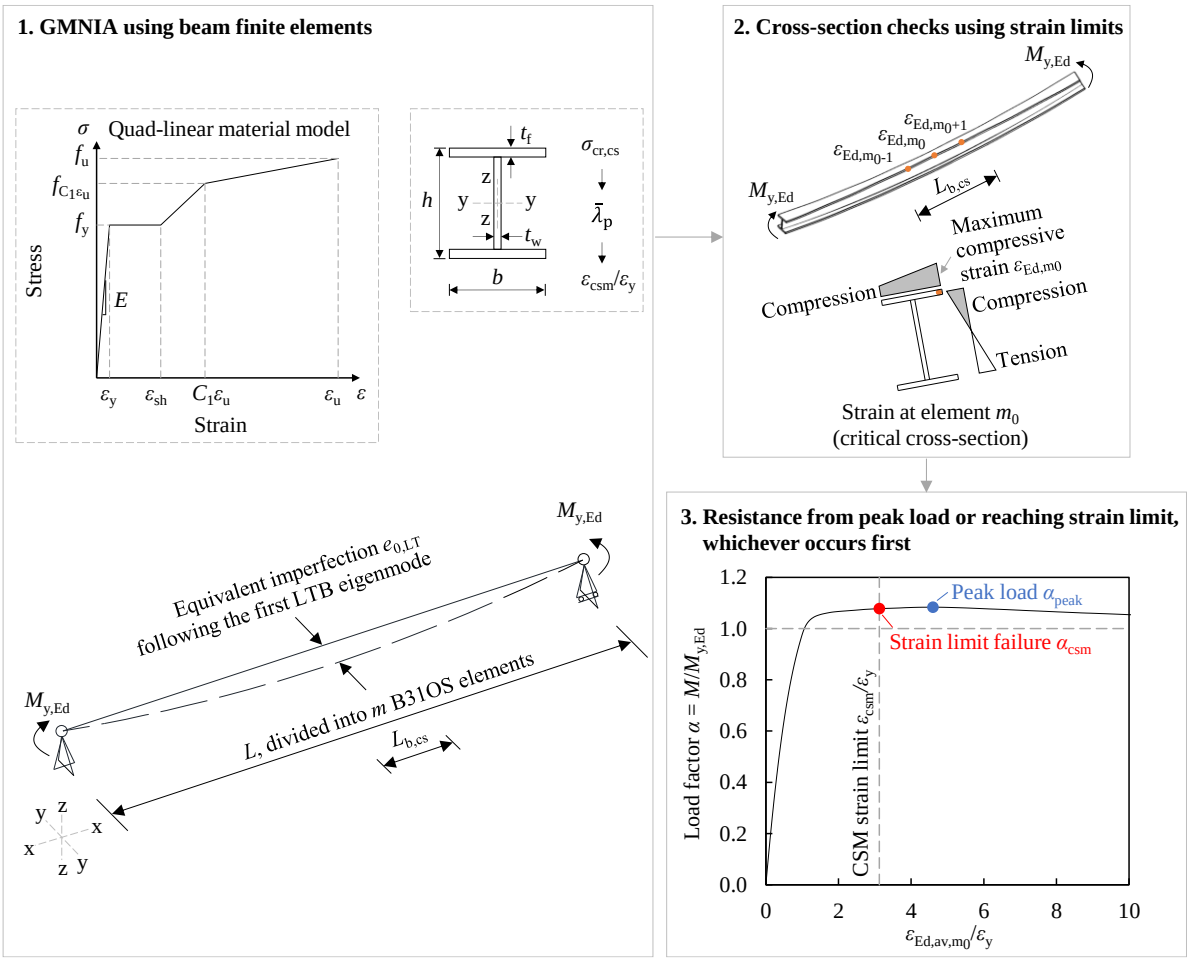

Figures

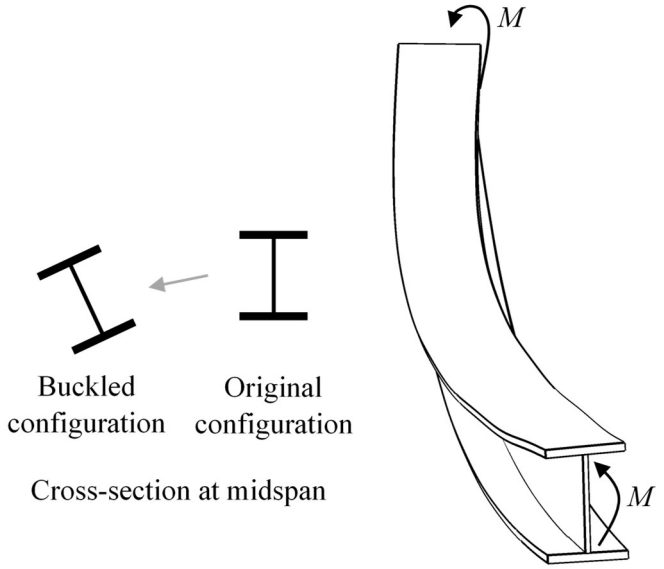

Fig. 1 I-section beam undergoing lateral-torsional buckling under uniform bending

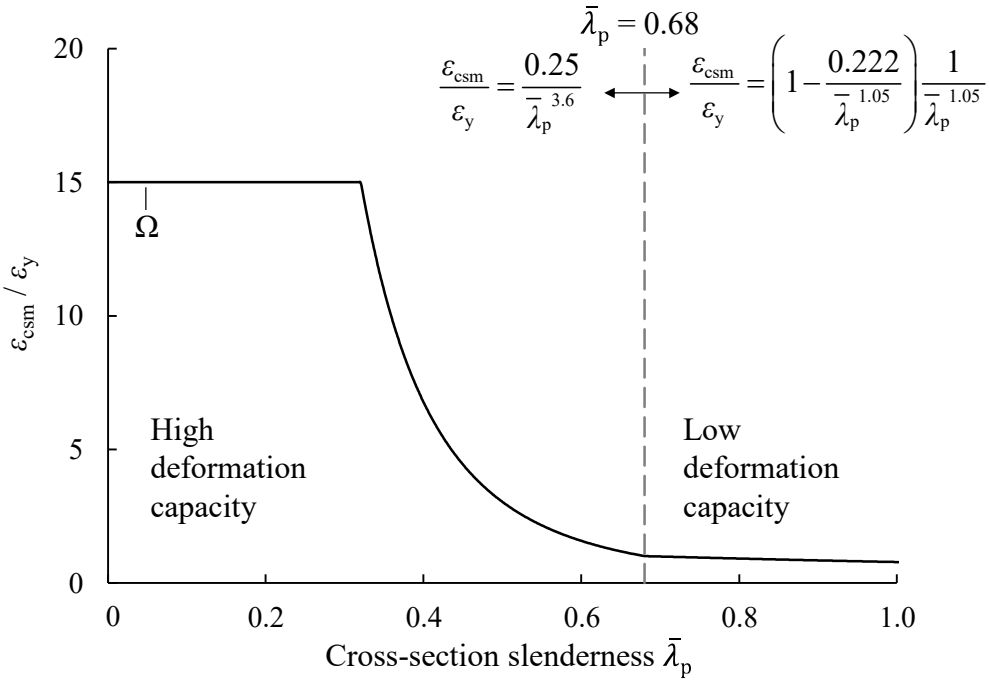

Fig. 2 CSM base curve: a continuous relationship between the cross-section slenderness $\bar{\lambda}_p$ and its deformation capacity expressed by the normalised limiting strain $\varepsilon_{csm}/\varepsilon_y$.

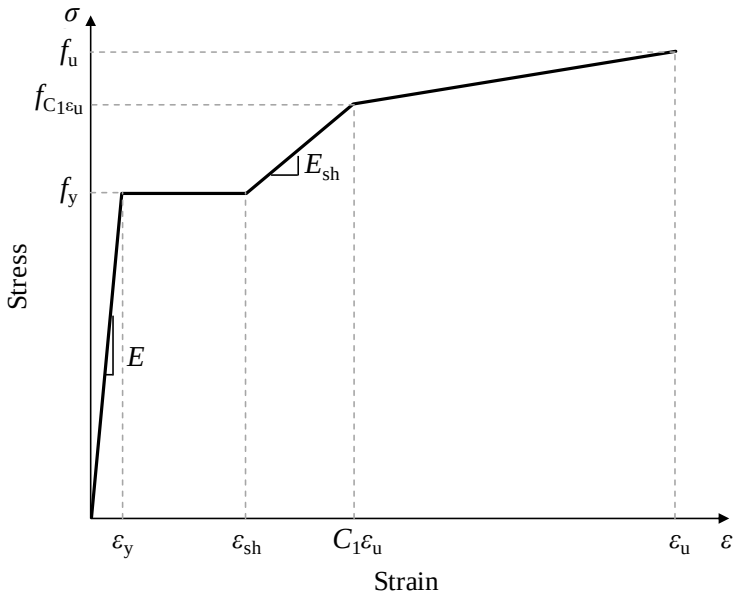

Fig. 3 Quad-linear material model for hot-rolled steel adopted in this study [43]

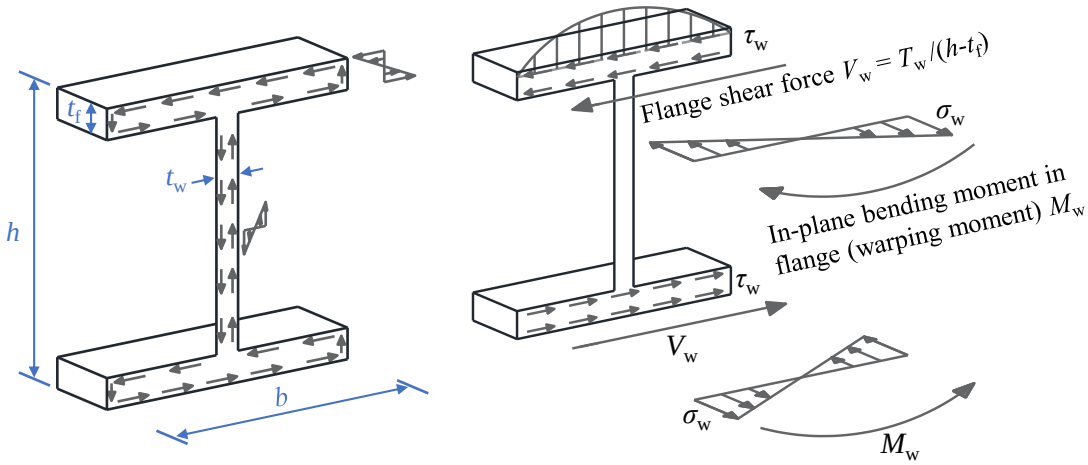

(a) Shear stresses due to St. Venant torsion τ_{St} (b) Normal stresses and shear stresses due to warping torsion σ_w and τ_w

Fig. 4 Shear stress and normal stress distributions due to (a) St. Venant torsion and (b) warping torsion

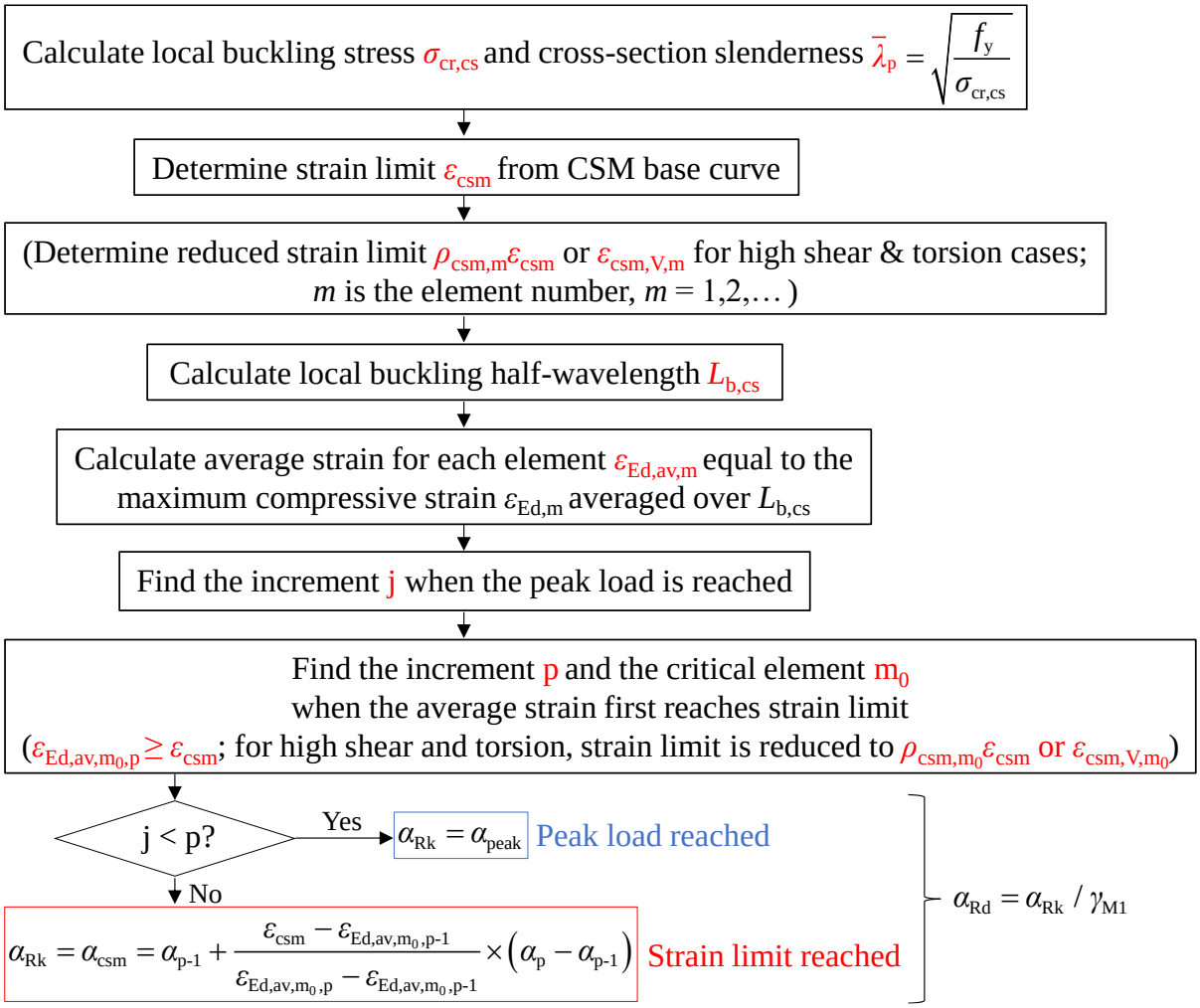

Fig. 5 Procedure to apply the proposed method of design by advanced analysis with CSM strain limits using beam elements to steel beams susceptible to LTB (where α_p is the load factor at increment p)

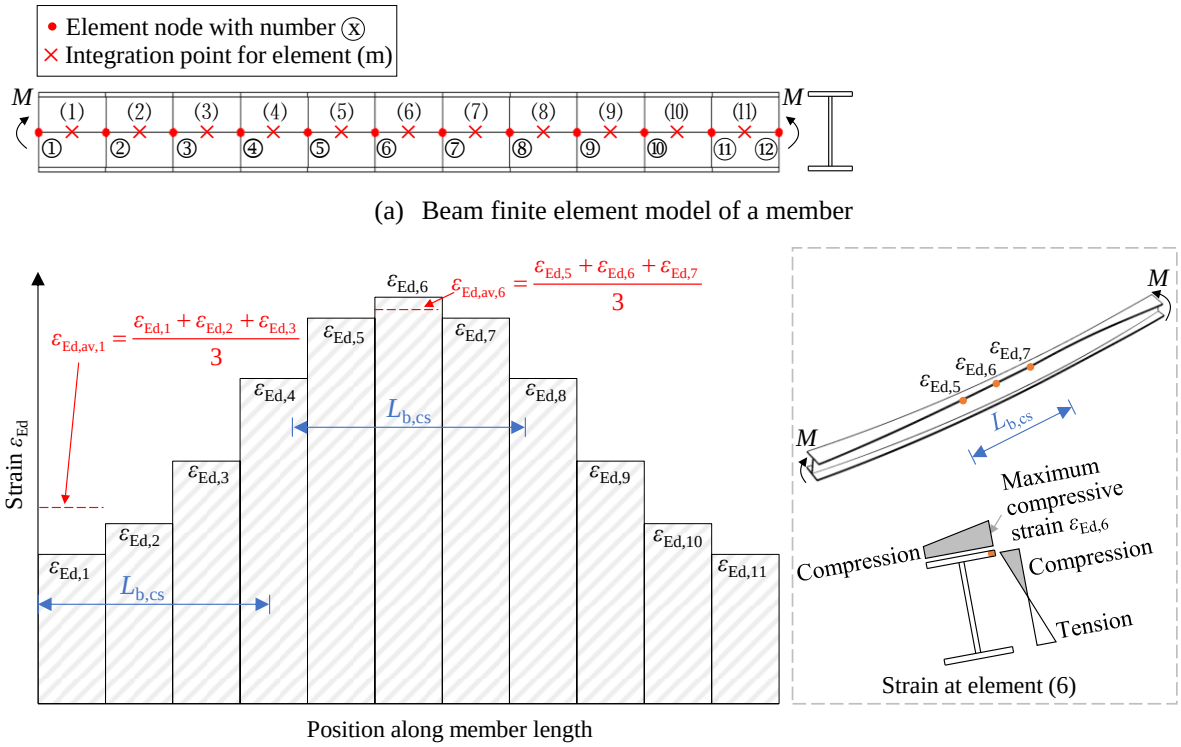

(a) Beam finite element model of a member

(b) Strain distribution along the member length

Fig. 6 Schematic representation of the strain averaging approach along a member with 11 beam elements; the average strains for elements 1 and 6, $\varepsilon_{Ed,av,1}$ and $\varepsilon_{Ed,av,6}$ respectively, are shown.

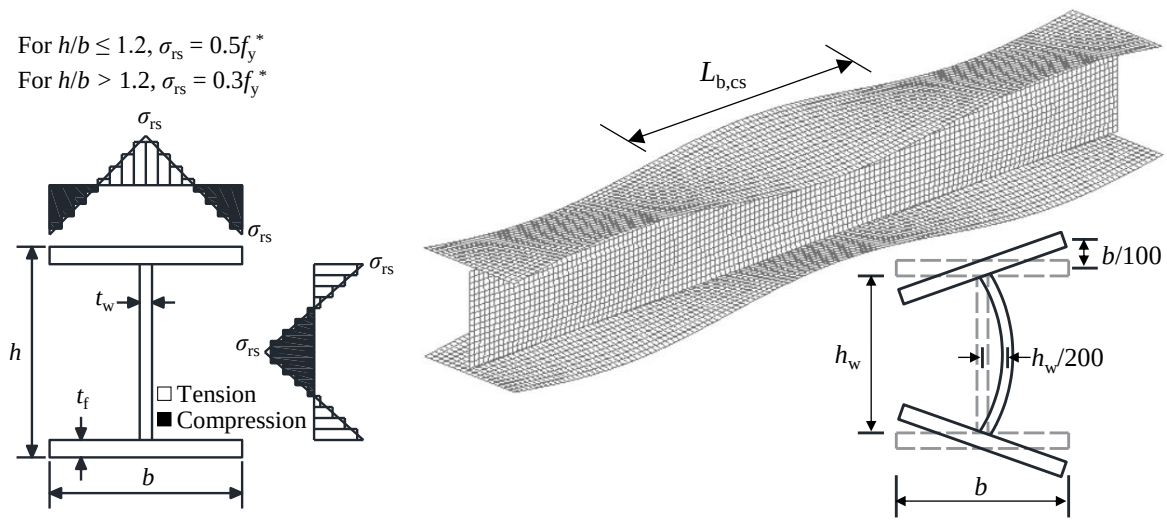

(a) Residual stresses

(b) Local geometric imperfections

Fig. 7 (a) Residual stress pattern and (b) local geometric imperfections applied to shell finite element models; note that $f_y^* = 235$ MPa.

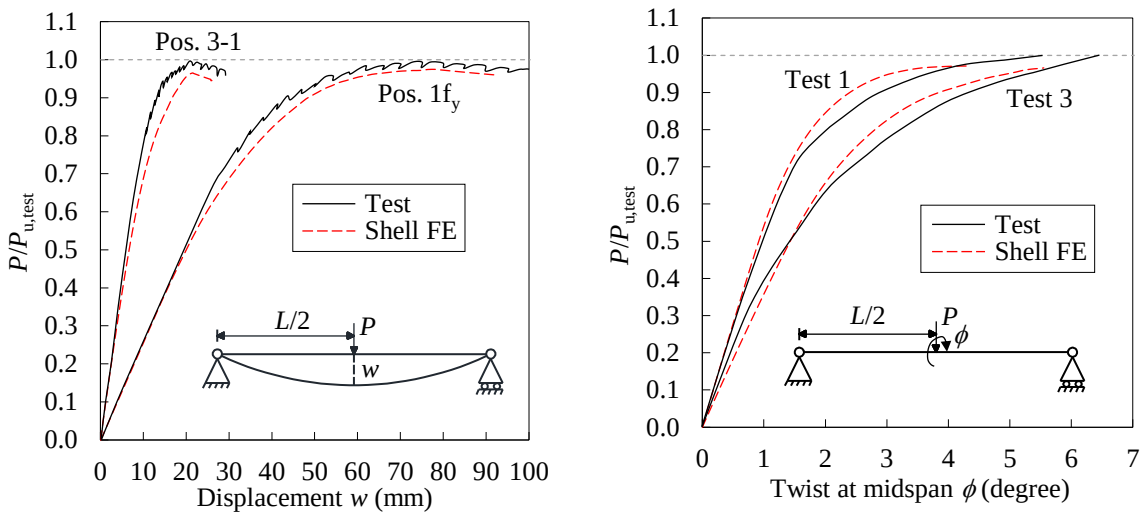

(a) Specimens Pos. 3-1 and Pos. 1f$_y$ tested in [65]

(b) Specimens Test 1 and Test 3 tested in [66,67]

Fig. 8 Comparison of experimental and numerical load-deformation curves of steel beams subjected to 3-point bending with eccentrically applied vertical loading at midspan, tested in [65] and [66,67]

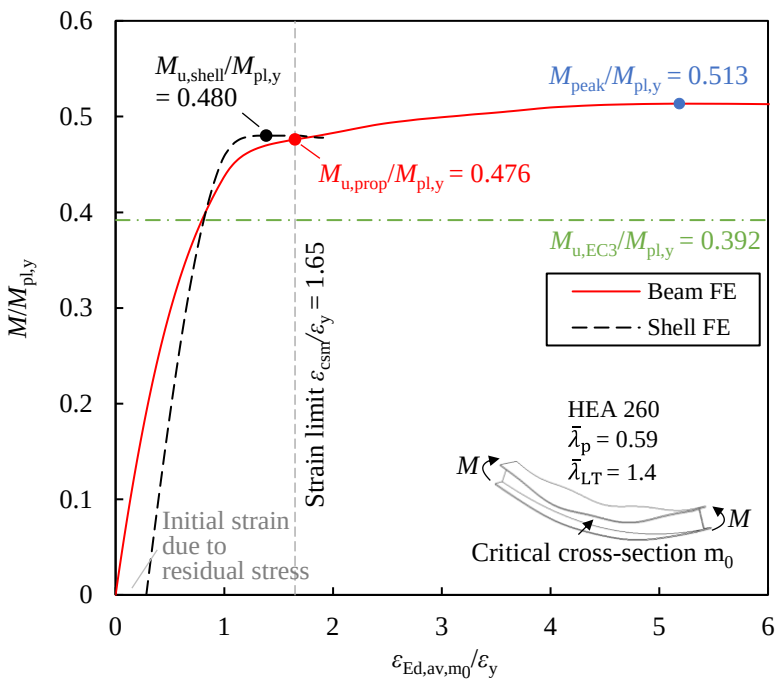

Fig. 9 Illustrative example of the application of the proposed method of design by advanced analysis with strain limits to a steel beam with an HEA 260 cross-section and non-dimensional LTB slenderness $\bar{\lambda}_{LT}$ of 1.4 under uniform bending

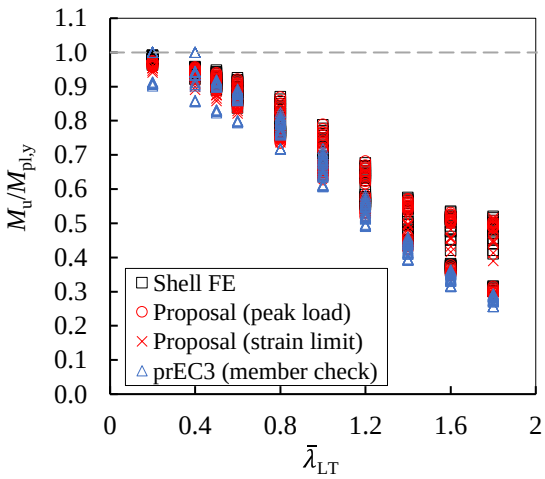

Fig. 10 Normalised ultimate bending moment capacities of steel beams under uniform bending obtained using the shell finite element models, proposed design method and prEN 1993-1-1

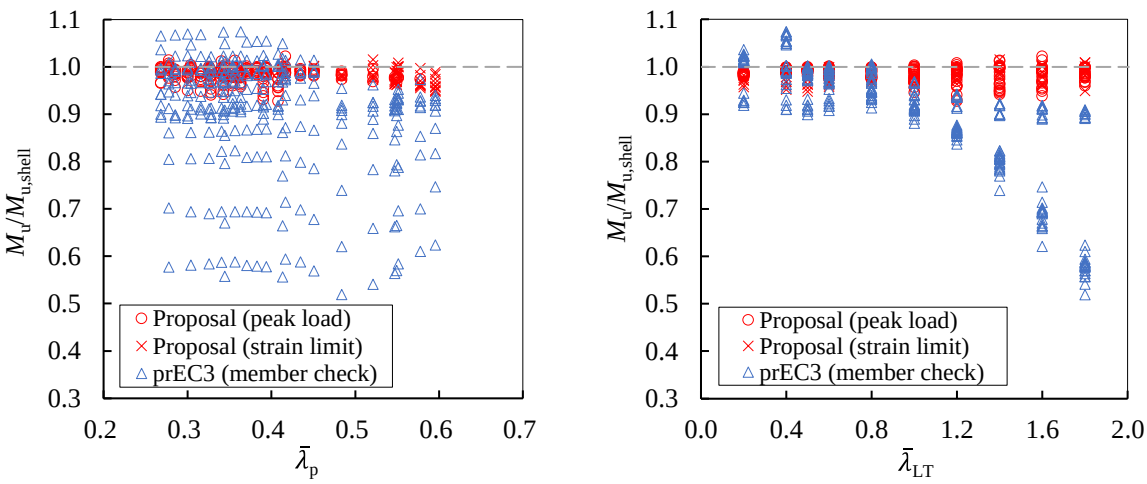

(a) Comparison of $M_u/M_{u,shell}$ obtained using the proposed method and prEN 1993-1-1 versus $\bar{\lambda}_p$

(b) Comparison of $M_u/M_{u,shell}$ obtained using the proposed method and prEN 1993-1-1 versus $\bar{\lambda}_{LT}$

Fig. 11 Comparison of the ratios of the ultimate bending moment capacities obtained using the proposed design approach and prEN 1993-1-1 to those obtained from the benchmark shell finite element models versus (a) cross-section slenderness $\bar{\lambda}_p$ and (b) LTB slenderness $\bar{\lambda}_{LT}$ for beams under uniform bending

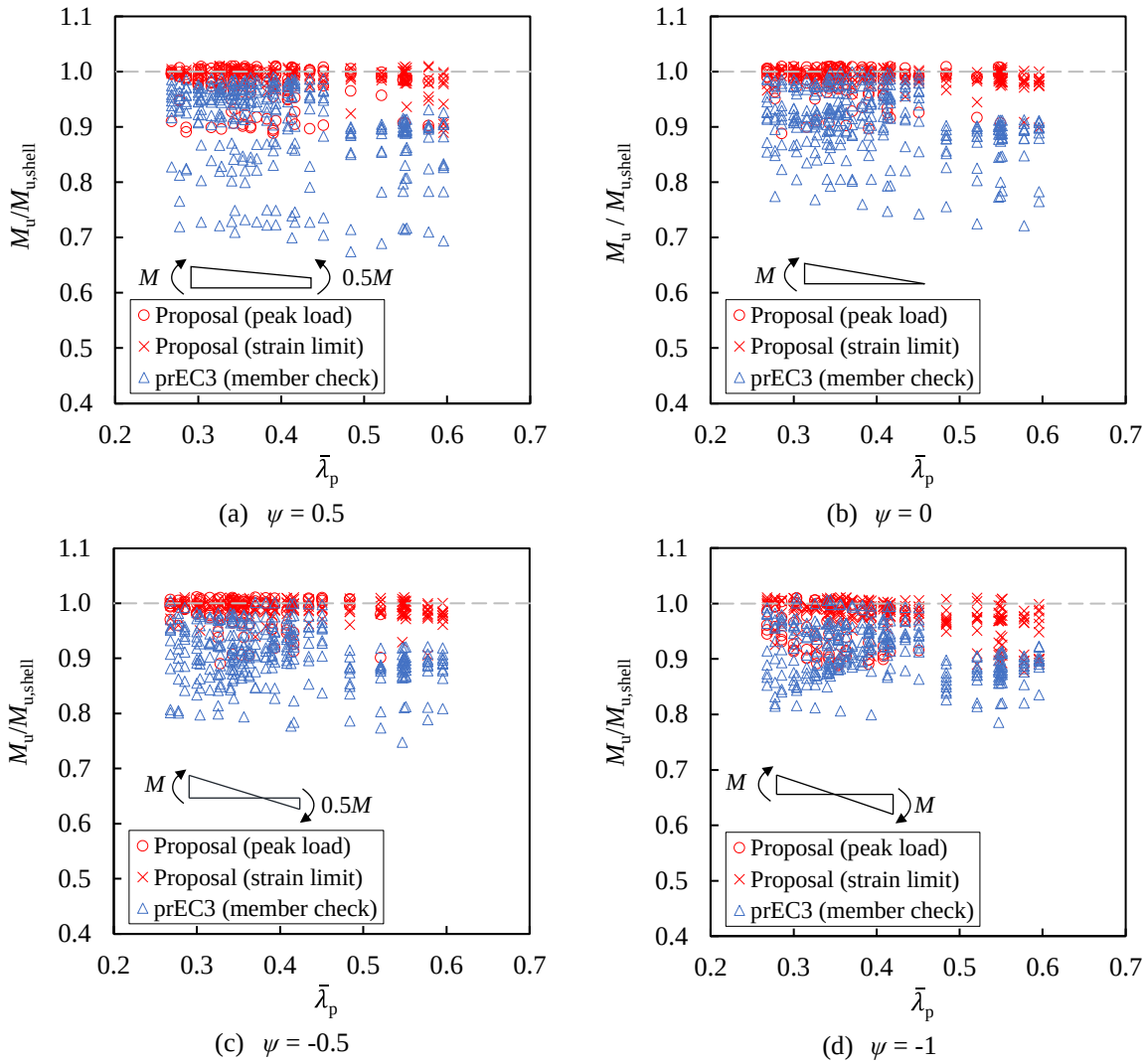

Fig. 12 Comparison of the ratios of the ultimate bending moment capacities obtained using the proposed design approach and prEN 1993-1-1 to those obtained from the benchmark shell element models versus cross-section slenderness $\bar{\lambda}_p$ for steel beams under non-uniform bending

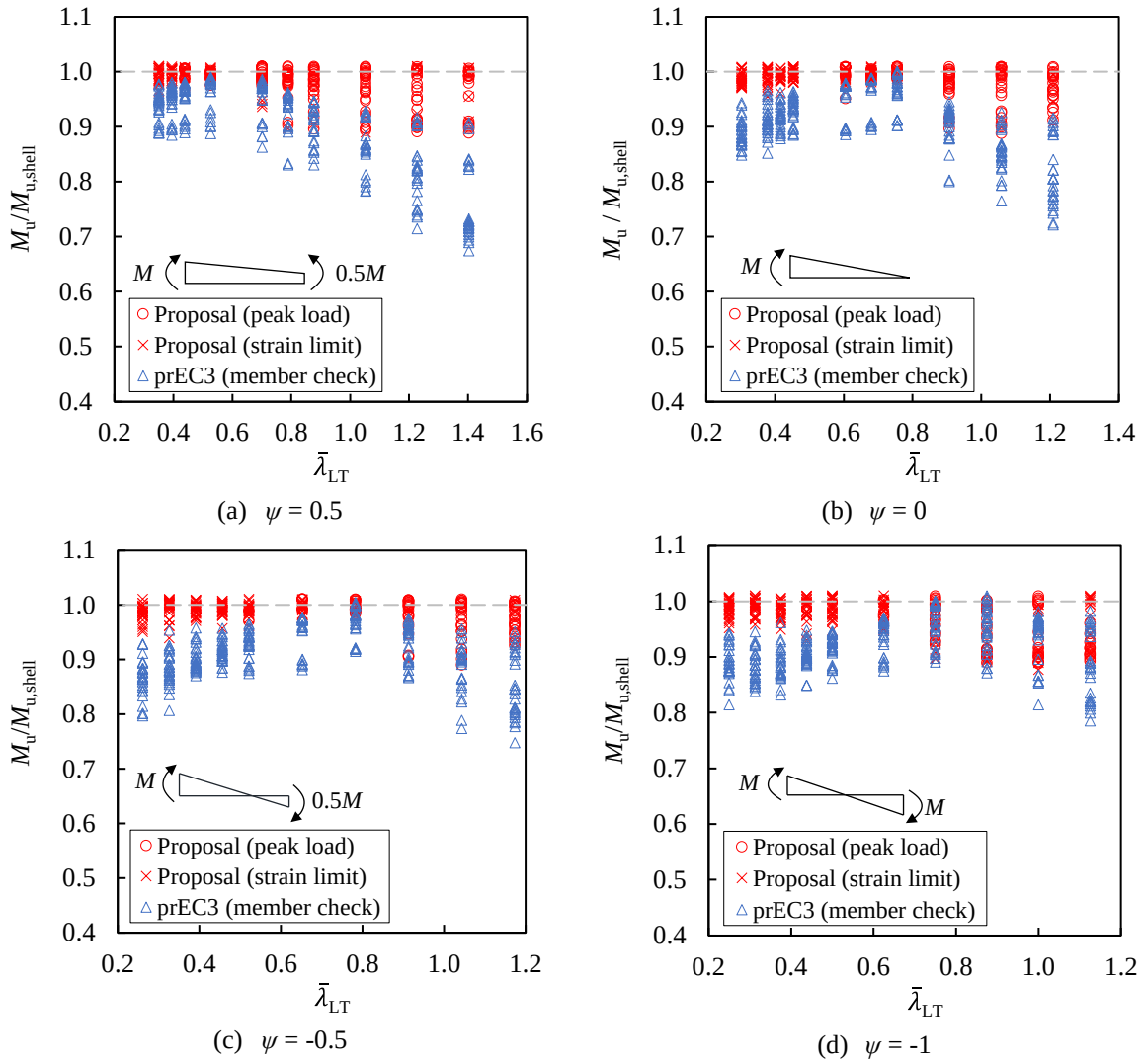

Fig. 13 Comparison of the ratios of the ultimate bending moment capacities obtained using the proposed design approach and prEN 1993-1-1 to those obtained from the benchmark shell element models versus member slenderness for LTB $\bar{\lambda}_{LT}$ for steel beams under non-uniform bending

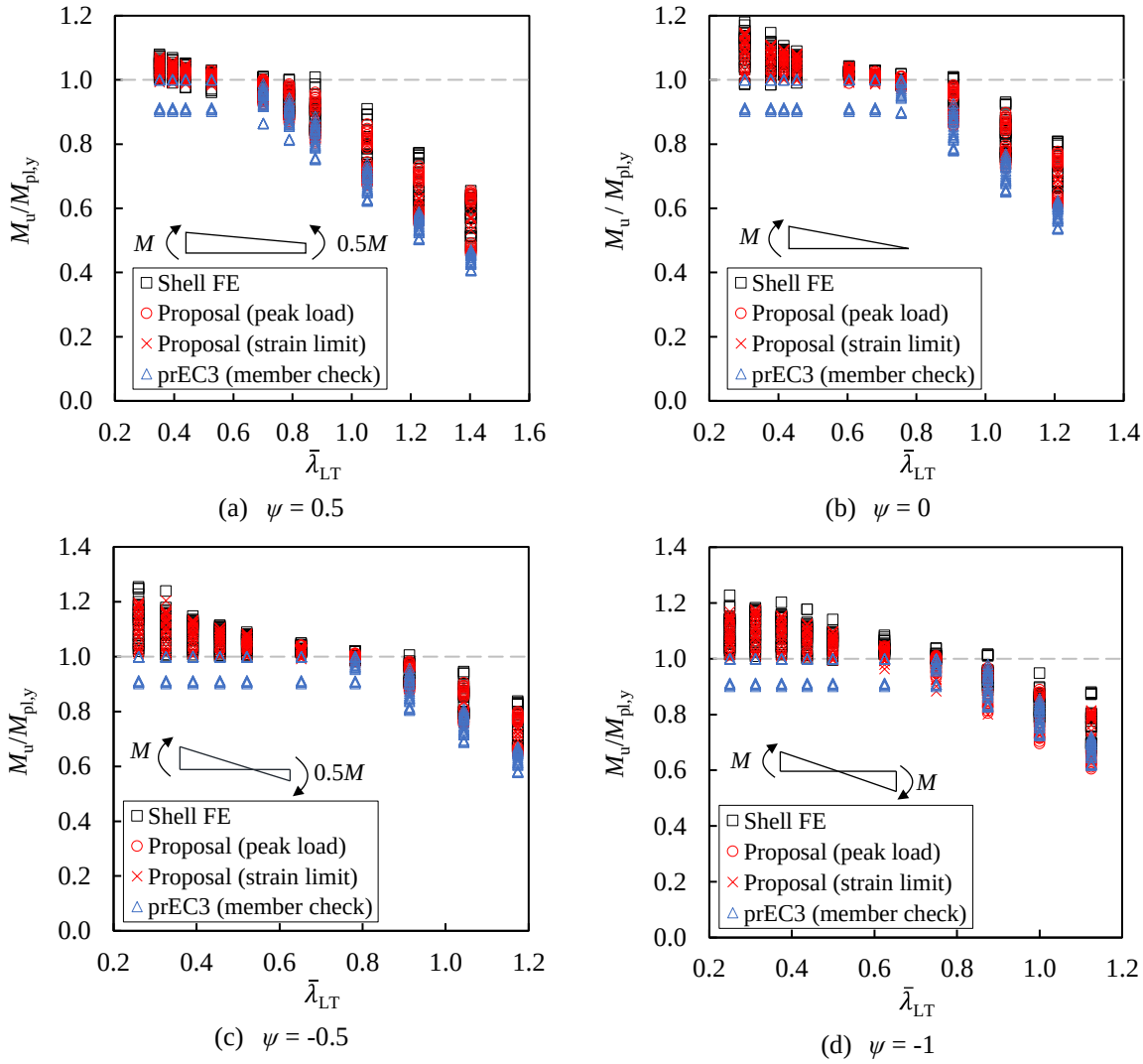

Fig. 14 Normalised ultimate bending moment capacities of steel members under non-uniform bending obtained from the proposed design method, shell FE models and prEN 1993-1-1 versus member slenderness for LTB $\bar{\lambda}_{LT}$

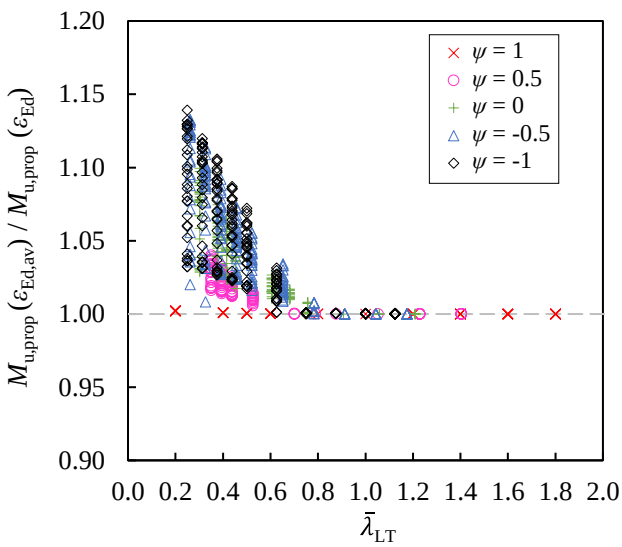

Fig. 15 Ratios between the ultimate bending capacities determined using the proposed design method with strain averaging (using $\varepsilon_{Ed,av}$) and without strain averaging (using ε_{Ed})

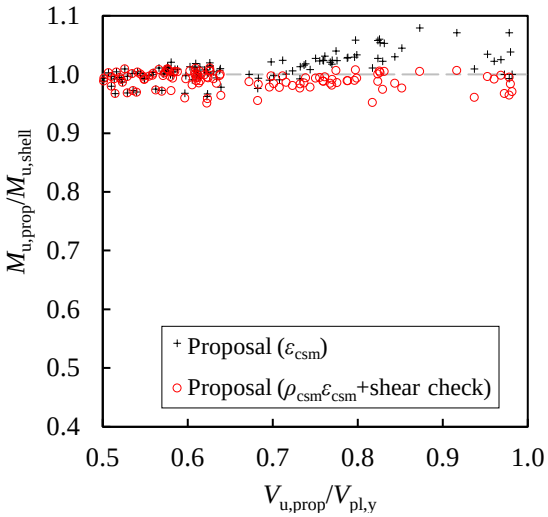

Fig. 16 Comparison between the ultimate bending moment capacities of steel beams under high shear predicted using the proposed design method with unreduced strain limit ε_{csm} and with reduced strain limit $\rho_{csm}\varepsilon_{csm}$ plus shear check against the shell FE results

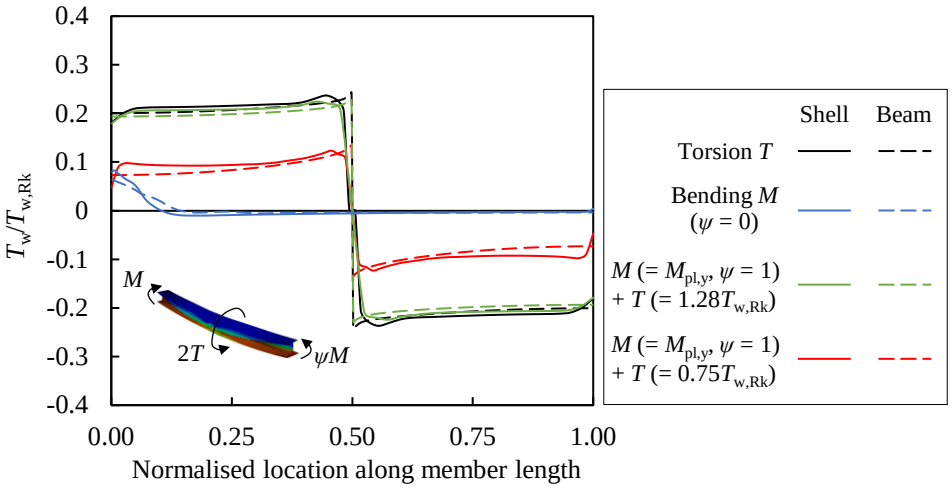

Fig. 17 Comparison of the normalised warping moment determined from beam FE models against those from shell FE models for pure torsion, pure bending and combined bending and torsion cases

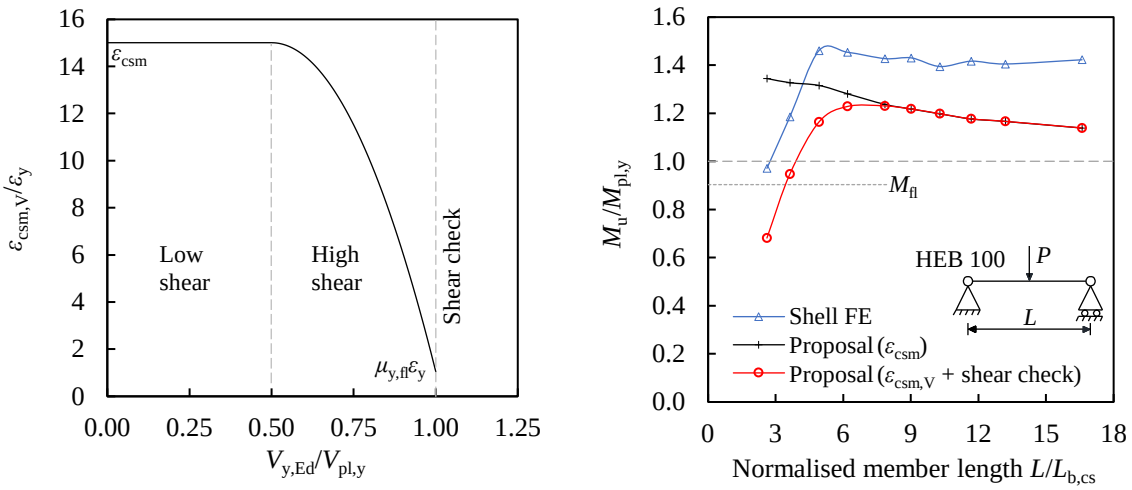

(a) Reduced CSM strain limit $\varepsilon_{csm,V}$

(b) Ultimate member capacity obtained from shell FE models and proposed design method

Fig. 18 (a) Reduced CSM strain limit $\varepsilon_{csm,V}$ and (b) ultimate member capacity of members made of grade S355 steel and with HEB 100 cross-section subjected to in-plane 3-point major axis bending obtained from shell FE models and proposed design method with unreduced ε_{csm} and reduced $\varepsilon_{csm,V}$ CSM strain limits plus shear check

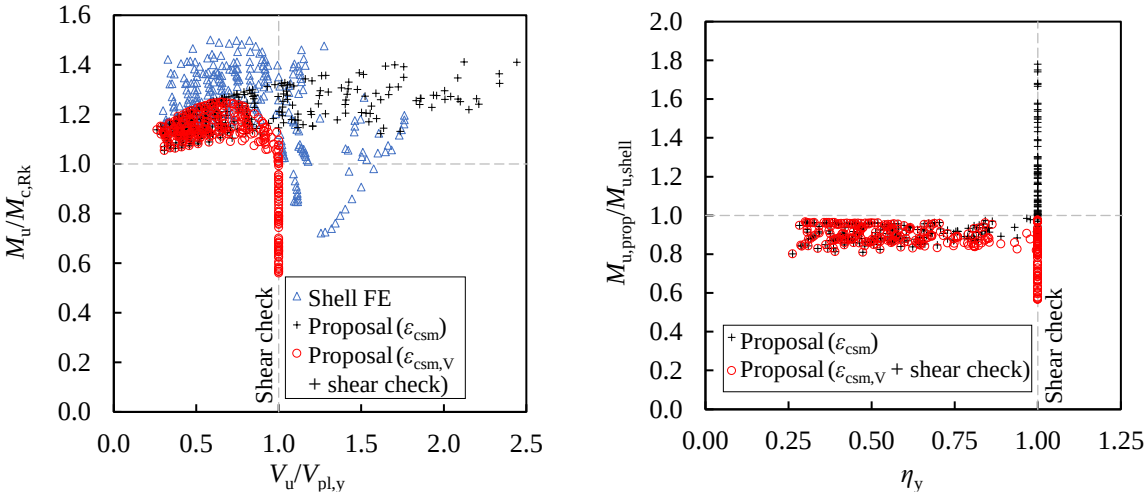

(a) Ultimate member capacity obtained from shell FE models and proposed design method using ε_{csm} and $\varepsilon_{csm,V}$ plus shear check

(b) Comparison between member capacities obtained from proposed method using ε_{csm} and $\varepsilon_{csm,V}$ plus shear check normalised by shell FE results

Fig. 19 Comparison between the ultimate member capacities of I-section members subjected to in-plane 3-point major axis bending obtained from shell FE models and proposed design method using unreduced ε_{csm} and reduced $\varepsilon_{csm,V}$ CSM strain limits plus shear check

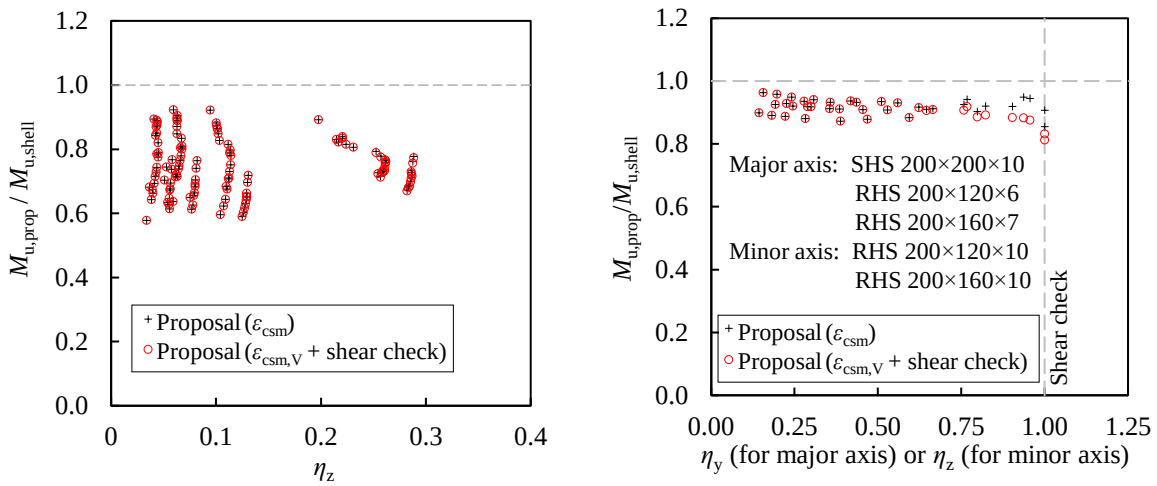

(a) 3-point minor axis bending of I-section members

(b) 3-point major/minor axis bending of SHS/RHS members

Fig. 20 Comparison between member capacity predictions obtained using ε_{csm} and $\varepsilon_{csm,V}$ plus shear check normalised by shell FE results for (a) I-section members subjected to 3-point minor axis bending and (b) SHS/RHS members subjected to 3-point major or minor axis bending

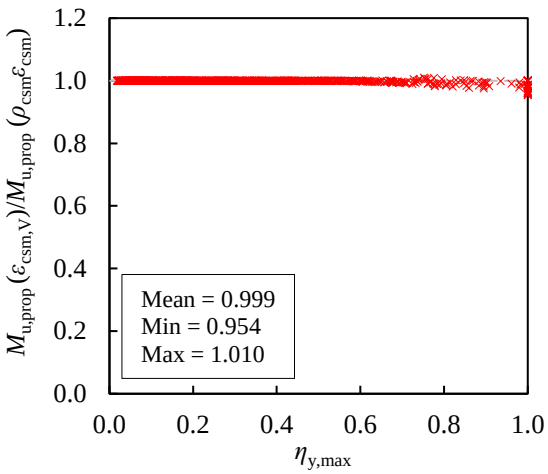

Fig. 21 Comparison between the ultimate member capacities obtained from proposed design method using the reduced strain limit considering high shear-torsion effects proposed in this study $\varepsilon_{csm,V}$ and the reduced strain limit proposed in [31] $\rho_{csm}\varepsilon_{csm}$ only considering shear effects due to shear force for all studied beams subjected to non-uniform bending

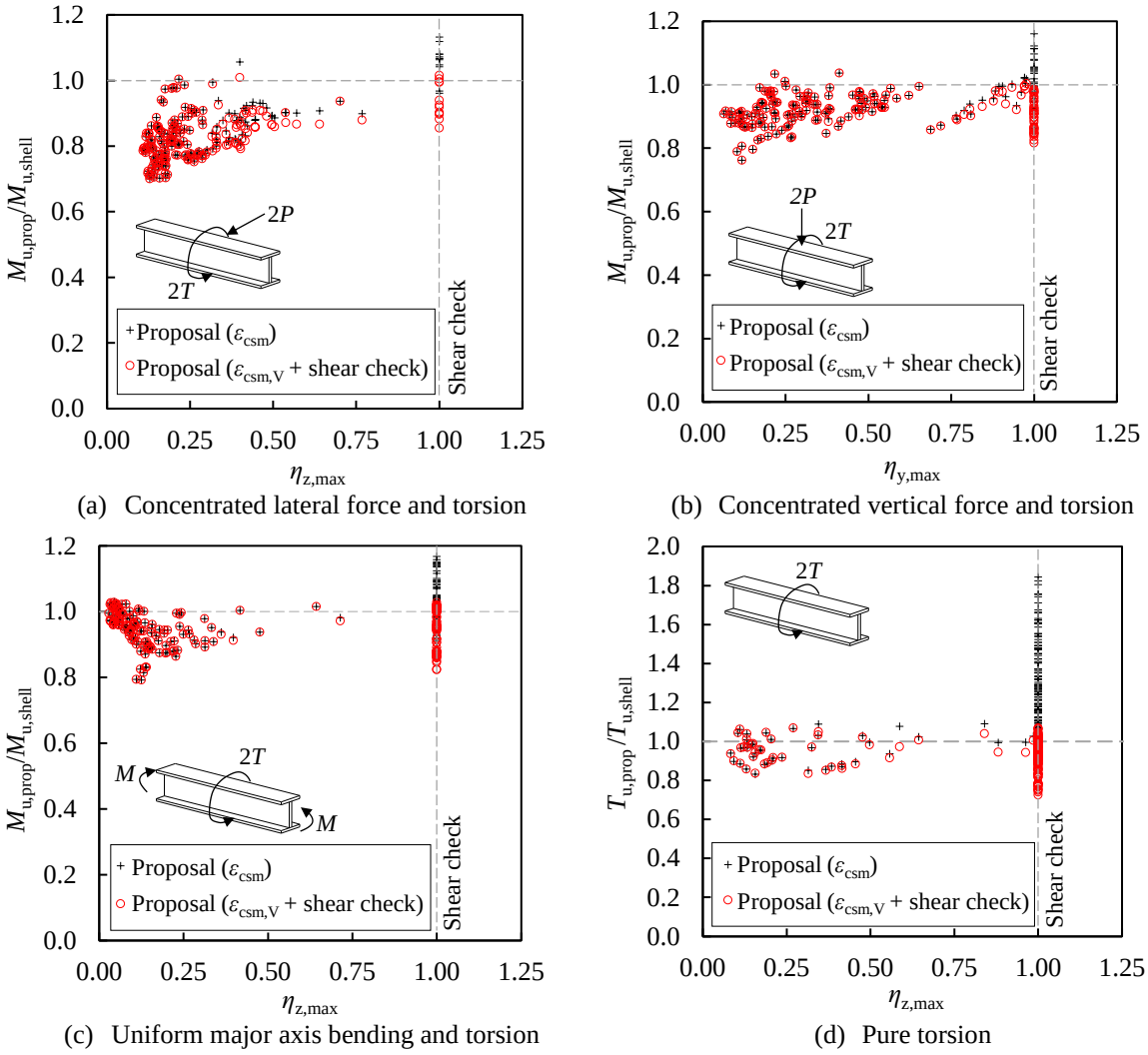

(a) Concentrated lateral force and torsion (b) Concentrated vertical force and torsion

(c) Uniform major axis bending and torsion (d) Pure torsion

Fig. 22 Comparisons between the ultimate capacity predictions determined through the proposed method using unreduced ε_{csm} and reduced $\varepsilon_{csm,V}$ CSM strain limits plus shear check normalised by benchmark shell FE results for I-section members subjected to (a) concentrated lateral force and torsion, (b) concentrated vertical force and torsion, (c) uniform bending and torsion and (d) pure torsion

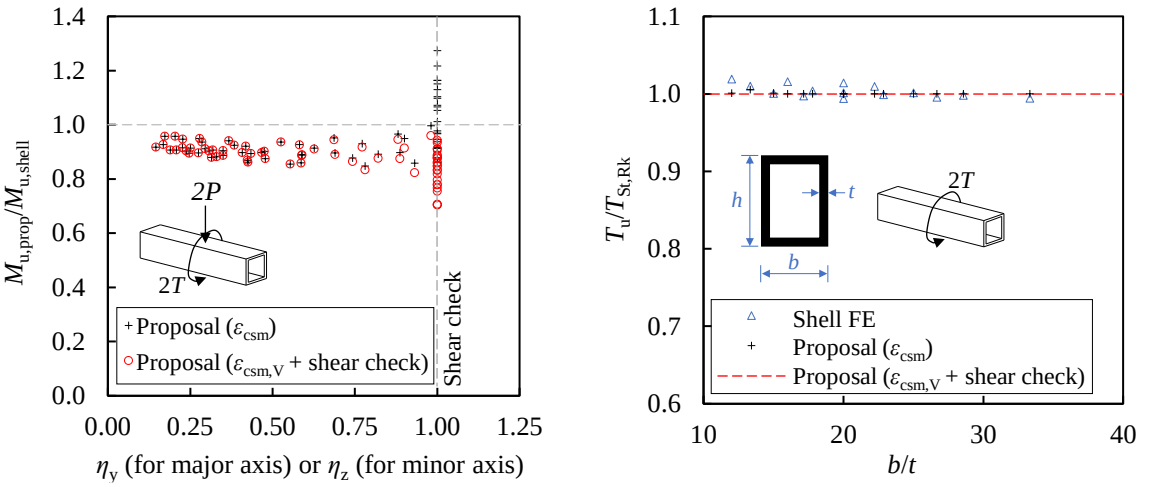

(a) Concentrated force and torsion (b) Pure torsion

Fig. 23 Comparisons between the ultimate capacity predictions determined through the proposed method using unreduced ε_{csm} and reduced $\varepsilon_{csm,V}$ CSM strain limits plus shear check against benchmark shell FE results of SHS/RHS members subjected to (a) concentrated vertical or lateral force and torsion and (b) pure torsion

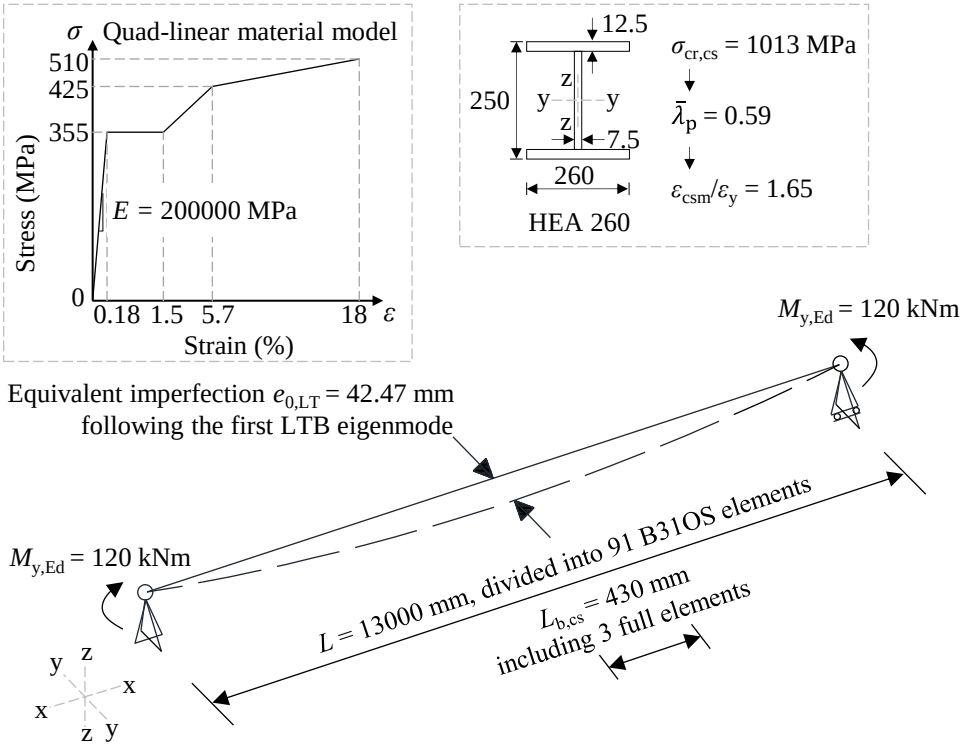

(a) Application of the proposed design method

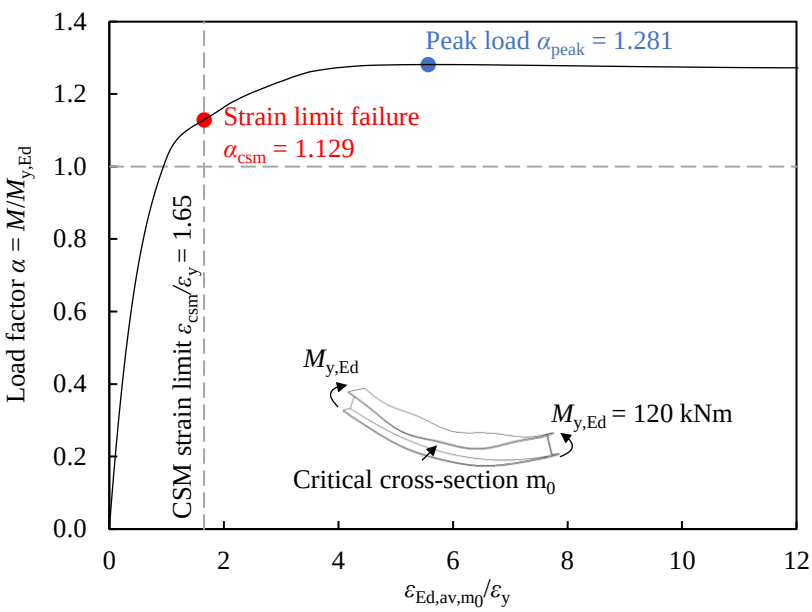

(b) Load path and load factors at the attainment of peak load factor and CSM strain limit ε_{csm}

Fig. 24 Worked example: design of a hot-rolled steel beam made of grade S355 steel with an HEA 260 cross-section (dimensions shown in mm) under uniform bending

Tables

Table 1 Summary of validation study for shell finite element models against experimental results from literature

Reference	Load configuration	No. of tests	$\alpha_{u,shell}/\alpha_{u,test}$	
			Mean	CoV
Dux & Kitipornchai (1983) [62]	3-point bending; 4-point bending	9	0.959	0.020
Ozbasaran et al. (2015) [63]	cantilever beams	9	0.921	0.068
Demirhan et al. (2020) [64]	cantilever beams	9	1.075	0.127
Schaper et al. (2019) [65]	3-point bending with eccentricity	7	0.970	0.023
Tusnin & Prokic (2015) [66,67]	3-point bending with eccentricity	6	0.901	0.061
Estabrooks & Grondin (2008) [68]	3-point bending with eccentricity	6	0.982	0.015
Lindner & Glitsch (2004) [69]	3-point bending with eccentricity	13	0.969	0.027
Total		59	0.971	0.084

Table 2 Summary of parameters considered in parametric studies and accuracy of proposed design method and prEN 1993-1-1 relative to results of benchmark shell FE models for steel beams under uniform and non-uniform bending

Moment ratio	Member slenderness	Cross-section	Cross-section slenderness	No. of cases	Design method	$M_u/M_{u,shell}$			
ψ	$\bar{\lambda}_{LT}$		$\bar{\lambda}_p$	N		Mean	CoV	Max	Min
1	0.20 – 1.80	10 IPE 10 HEB 10 HEA	0.26 – 0.60	300	Proposed	0.984	0.016	1.022	0.928
					prEC3	0.901	0.137	1.074	0.519
0.5	0.35 – 1.40			300	Proposed	0.982	0.031	1.010	0.889
					prEC3	0.904	0.085	0.990	0.674
0	0.30 – 1.21			300	Proposed	0.988	0.022	1.010	0.888
					prEC3	0.910	0.063	1.000	0.721
-0.5	0.26 – 1.17			300	Proposed	0.989	0.021	1.011	0.891
					prEC3	0.908	0.054	1.005	0.748
-1	0.25 – 1.13			300	Proposed	0.971	0.036	1.011	0.877
					prEC3	0.914	0.051	1.010	0.786
Total				1500	Proposed	0.983	0.027	1.022	0.877
					prEC3	0.907	0.084	1.074	0.519

Table 3 Shear stress distribution across plate thickness of different types of cross-sections subjected to vertical shear force $V_{y,Ed}$, lateral shear force $V_{z,Ed}$ and torsion moment T_{Ed}

I-section	Channel section	SHS/RHS
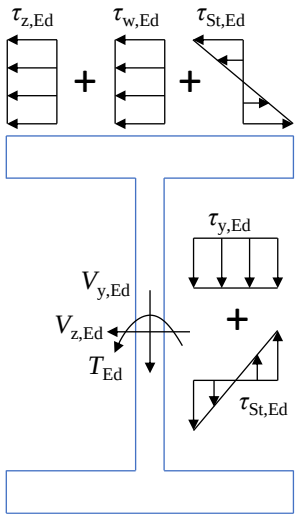	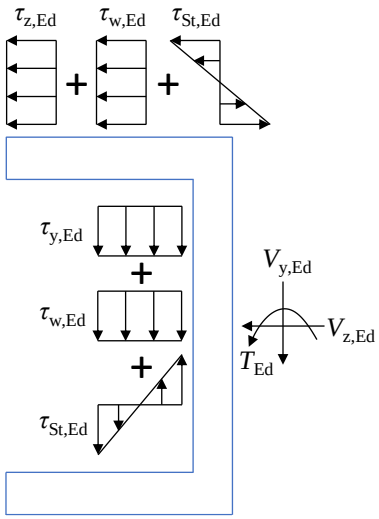	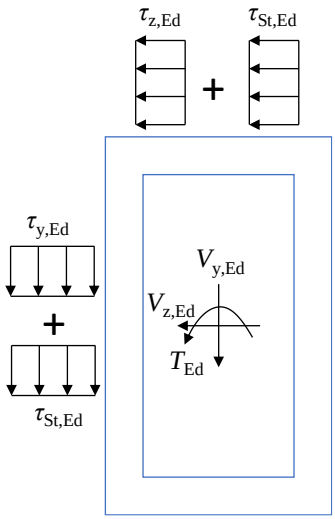

Table 4 Expressions for calculating the factors η_y and η_z for considering the combined effects of shear stresses due to shear force and torsion for different types of cross-sections

	Major axis bending	Minor axis bending
I-section	$\eta_y = \dfrac{V_{y,Ed}}{\sqrt{1-\dfrac{T_{St,Ed}}{T_{St,Rk}}}V_{y,Rk}} \le 1$	$\eta_z = \dfrac{V_{z,Ed}}{\sqrt{1-\dfrac{T_{St,Ed}}{T_{St,Rk}}}V_{z,Rk}} + \dfrac{T_{w,Ed}}{\sqrt{1-\dfrac{T_{St,Ed}}{T_{St,Rk}}}T_{w,Rk}} \le 1$
Channel section	$\eta_y = \dfrac{V_{y,Ed}}{\sqrt{1-\dfrac{T_{St,Ed}}{T_{St,Rk}}}V_{y,Rk}} + \dfrac{T_{w,Ed}}{\sqrt{1-\dfrac{T_{St,Ed}}{T_{St,Rk}}}T_{w,Rk}} \le 1$	$\eta_z = \dfrac{V_{z,Ed}}{\sqrt{1-\dfrac{T_{St,Ed}}{T_{St,Rk}}}V_{z,Rk}} + \dfrac{T_{w,Ed}}{\sqrt{1-\dfrac{T_{St,Ed}}{T_{St,Rk}}}T_{w,Rk}} \le 1$
SHS/RHS	$\eta_y = \dfrac{V_{y,Ed}}{\left(1-\dfrac{T_{St,Ed}}{T_{St,Rk}}\right)V_{y,Rk}} \le 1$	$\eta_z = \dfrac{V_{z,Ed}}{\left(1-\dfrac{T_{St,Ed}}{T_{St,Rk}}\right)V_{z,Rk}} \le 1$